300

UCRL-8059
Chemistry Distribution

UNIVERSITY OF CALIFORNIA

Radiation Laboratory
Berkeley, California

Contract No. W-7405-eng-48

THE KINETICS OF THE COMPLEXING OF FERRIC ION BY THIOCYANATE AND CHLORIDE IONS

Claude Peter Coppel

December 1957

(Ph.D. Thesis)

Printed for the U. S. Atomic Energy Commission

DISCLAIMER

THE KINETICS OF THE COMPLEXING OF FERRIC ION BY THIOCYANATE AND CHLORIDE IONS

Contents

Contents (Cont'd)

THE KINETICS OF THE COMPLEXING OF FERRIC ION BY THIOCYANATE AND CHLORIDE IONS

Claude Peter Coppel

Radiation Laboratory and
Department of Chemistry and Chemical Engineering
University of California, Berkeley, California

December 1957

ABSTRACT

An apparatus for rapidly mixing two solutions and recording the light absorption, which was developed by Connick and Below,[1] has been modified. The mixing characteristics have been studied and models have been developed in an attempt to understand the observed mixing phenomena.

The apparatus has been applied to a study of the kinetics of the reactions

$$Fe^{+++} + SCN^{-} = FeSCN^{++},$$

$$Fe^{+++} + Cl^{-} = FeCl^{++}$$

in aqueous solution, with both reactions having the forward rate law

$$\frac{d(FeX^{++})}{dt} = k_1(Fe^{+++})(X^{-}) + k_2 \frac{(Fe^{+++})(X^{-})}{(H^{+})},$$

where X^{-} represents either SCN^{-} or Cl^{-}.

The rate constants k_1 and k_2 have been measured as a function of temperature, and the heats and entropies of activation have been calculated. Mechanisms for the observed rate law have been discussed and the entropies of activation have been compared with those for analogous

reaction rates and with some equilibrium entropies of complexing.

A rate for chloride complexing of ferric ion has been obtained from nuclear magnetic resonance studies and compared with the results of the spectrophotometric kinetic study.

THE KINETICS OF THE COMPLEXING OF FERRIC ION BY THIOCYANATE AND CHLORIDE IONS

Claude Peter Coppel

Radiation Laboratory and
Department of Chemistry and Chemical Engineering
University of California, Berkeley, California

December 1957

INTRODUCTION

In recent years Professor Robert E. Connick and Dr. John F. Below[1] have developed a rapid-mixing device and a rapid-recording spectrophotometer. These were successfully used in studying the rate law of the first ferric thiocyanate complex formation. The mixing apparatus was of the moving-baffle type, i.e., the reactants are initially separated by a baffle system, which can be removed rapidly, causing the reactants to mix because of the turbulence produced. Their apparatus was not well adapted for temperature-dependence studies; it was not thermostated nor did it have an internal temperature-measuring system. There was also a premixing problem, i.e., reactants mixed partially before the baffle was removed. The premixing was due primarily to the structural complexity of the baffle.

The work reported here is a continuation of this earlier study of rapid reactions and consists of (a) modifications in the apparatus; (b) calculations on certain mixing phenomena, in order to gain some insight into both the processes and the limitations of the mixing apparatus; (c) a temperature-dependence study of the kinetics of the ferric thiocyanate complexing reaction; and (d) a study of the kinetics of the ferric chloride complexing reaction.

Part I

APPARATUS AND CALCULATIONS

Experimental Description and Modifications

Introduction

This section contains a general description of the experimental apparatus and procedures. It should, perhaps, come logically after the section on mixing-phenomena calculations; however, it seemed that the reader would benefit in following the calculations by first being introduced to the general procedures and techniques of this study.

Mixer and Recording System

Only a brief description of the apparatus is given here. A more detailed discussion is available in Below's work.[1]

The details of construction of the mixing device are shown in Figs. 1 and 2. Except for the windows, all parts in contact with liquid were made of stainless steel. The metal walls were screwed together and the outside seams were soft-soldered. All outside seams were painted with Glyptal varnish and the interior was coated with "Harrisite,"* a phenolic resin which exhibits extreme chemical inertness to all common acidic reagents and is remarkably tough and tenacious. The removable base plate was sealed with a cork gasket and possessed two needle valves through which reactants could be admitted.

The baffles, shown in Figs. 2 and 2, were connected at the top to a hollow circular tube which transmitted the spring force, and at the bottom to the flat perforated turbulator plate.

---

*Harrisite and Chemical Company, Manitowoc, Wisconsin.

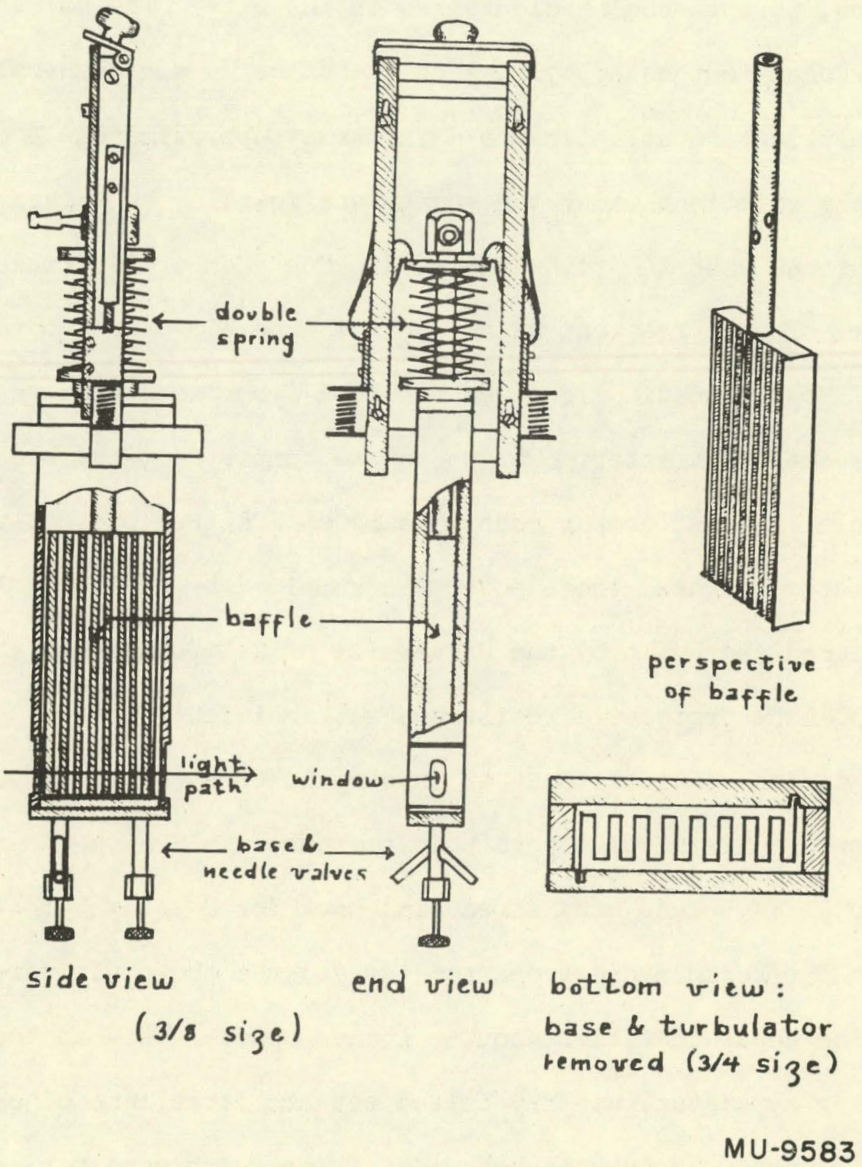

Fig. 1. The stainless steel moving-baffle mixer.

The top of the chamber included a mechanical device for cocking and releasing the coiled springs that actuated the baffle. A Hoke needle valve projected through the side of the chamber and supplied a means for producing a vacuum within the chamber.

The mixer was filled by drawing the reactants, contained in glass bulbs, through the needle valves in the base. The solutions were previously outgassed by shaking the bulbs on a mechanical shaker while submitting the solutions to a vacuum of approximately 3 cm. Evaporation of the solutions under the vacuum was found to be trivial for aqueous solutions with the technique used. The chamber was filled to contain 30 ml of each reactant with 55 ml of free air space above the solutions.

Monochromatic light was obtained from the optical system of a Beckman DU spectrophotometer. The phototube compartment had been replaced by a specially built compartment housing an RCA-1P28 photomultiplier tube and resistor network, whose power was supplied by an 1800-volt dc power supply, designed and built by the University of California Radiation Laboratory. A 330-kohm protective resistance was included in series. The output was fed to the vertical input of an oscilloscope (see later discussion). Mounted in front of the cathode-ray tube was a view camera with a 4-inch focus, f:4.5 lens, and a reducing back for 2-1/4 x 3-1/4-inch sheet film.

The Beckman spectrophotometer and the photomultiplier compartment sat on separate tables about 6 inches apart. Between these tables the mixing apparatus, stiffly bolted between large lead blocks, rested on a tall, narrow table 5 inches wide, filled with sand for added stability. This narrow table rested on the floor and was coupled to the other two tables only through sponge rubber pads which helped hold it erect, thus minimizing the effect on the optical components of the shock of firing the mixer.

Procedure

To make a kinetic run, the mixer was filled with the reactants and placed in position. The oscilloscope sweep frequency was adjusted with a known frequency to give two or three sweeps per half life of the substance whose absorbency was being measured. In the work described here, the sweep frequency varied between 6 and 60 cycles per second. The lens of the camera, set at maximum aperture, was uncapped and the coiled mixer springs released. After a second or two the lens was recapped. Super Panchro Press Type B film was used. The washed and dried negative was measured with a low-power microscope to obtain a concentration-versus-time curve. A typical negative is reproduced in Fig. 5 of Part II.

The Baffle

Fig. 1 shows the mixer as developed by Below.[1] The baffle had been designed in such a way as to divide the mixer into two regions of liquid, consisting of 18 laminae of the two solutions. The intention was to aid the mixing process by having the two reactants somewhat "mixed" before any actual mixing occurred. With this type of baffle it was necessary to have baffle-mixer seals along the entire vertical height of the mixing compartment. This was done by having flat plates projecting 1/8 inch on two sides of the baffle; these plates rode in the narrow grooves milled into the mixing compartment. These grooves are seen in the bottom view of Fig. 1. Tests on premixing indicated that it could only be caused by leakage around the groove seals, and it was concluded that a baffle that could eliminate this source of leakage would not have premixing troubles.

The design of the baffle used in the work reported herein is shown in Fig. 2. This baffle consists of a stainless steel rectangular box B, connected as before to a circular tube T and a perforated base plate P.

The box was of such dimensions that the volume within the baffle was equal to that which surrounded it. It served to separate the reactants, one within the box and one occupying the space between the box and the chamber walls. In this way reactants could premix only by leaking under the base plate, which was easily prevented by placing a neoprene gasket underneath the baffle and applying a small external pressure to the baffle until the reaction was started.

It is doubtful that this baffle mixes as efficiently as the one used by Below. Studies of mixing rates indicate 83% mixing in 16 milliseconds for this baffle as compared with 90% mixing in 12 to 15 milliseconds observed by Below. However, the elimination of the premixing problem was considered advantageous in comparison with the small loss in mixing rate. It is possible that one could increase the mixing rate somewhat with this type of baffle by increasing the velocity of the liquids by decreasing the orifice area; however, one is still limited by force input and orifice-flow limitations, as is discussed in a later section.

The new baffle also eliminated to some extent the corrosion problem. Corrosion was a serious limitation to Below, since any protective coating that he applied tended to chip off wherever sliding contact occurred, especially around the grooved slots. In the new baffle virtually no sliding contact is required, and chipping has been almost completely eliminated.

Oscilloscope Decay

The RCA-W056A oscilloscope that was originally used in the spectrophotometric recording system had an overshoot-decay characteristic. When a constant voltage was applied to the vertical input the initial displacement of the horizontal sweep was as much as 10% larger than its final

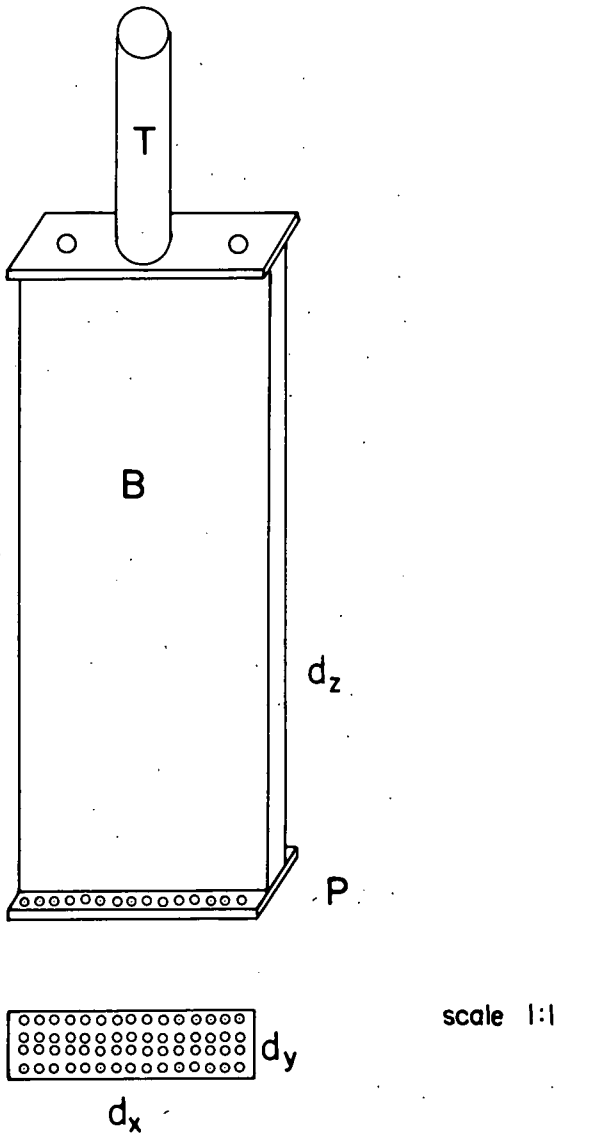

Fig. 2. The second baffle.

displacement, with the decay generally occurring over 2 to 3 seconds. The exact nature of the decay was complicated and in general not quantitatively reproducible. However, when maximum possible corrections for this effect were made on kinetic runs, the resulting changes were found to be negligible. This oscilloscope was used in all the work on the ferric thiocyanate system. In the ferric chloride work a DuMont 304-A oscilloscope was used; it had no observable decay characteristics.

The new oscilloscope also had a more linear response than the first oscilloscope. If the displacement were linear with percent transmission then the optical density would be given by $D = \log x_b/x$, where x_b and x refer to the displacement caused by the blank and by the sample with respect to the dark current on the oscilloscope screen. The linearity was checked by placing an absorption cell filled with potassium dichromate in the light path of the rapid-recording spectrophotometer and measuring the oscilloscope displacement at various concentrations of dichromate. The optical densities were then measured on a Cary Model 11 recording spectrophotometer. Fig. 3 shows a typical plot of $\log x_b/x$ versus D, which indicates D equal to $\log x_b/x$ within experimental error.

The response time of the oscilloscope was approximately 2 microseconds from 10% to 90% displacement, which in no way further limits the apparatus. Below had measured an over-all time constant of 10^{-5} second for the entire recording spectrophotometer.

Temperature Measurement

Below measured the temperatures of his solutions by removing a sample through one of the needle valves at the base of the mixer, and quickly measuring its temperature. In runs in which the solution temperature differed greatly from room temperature the receiving vessel and thermometer

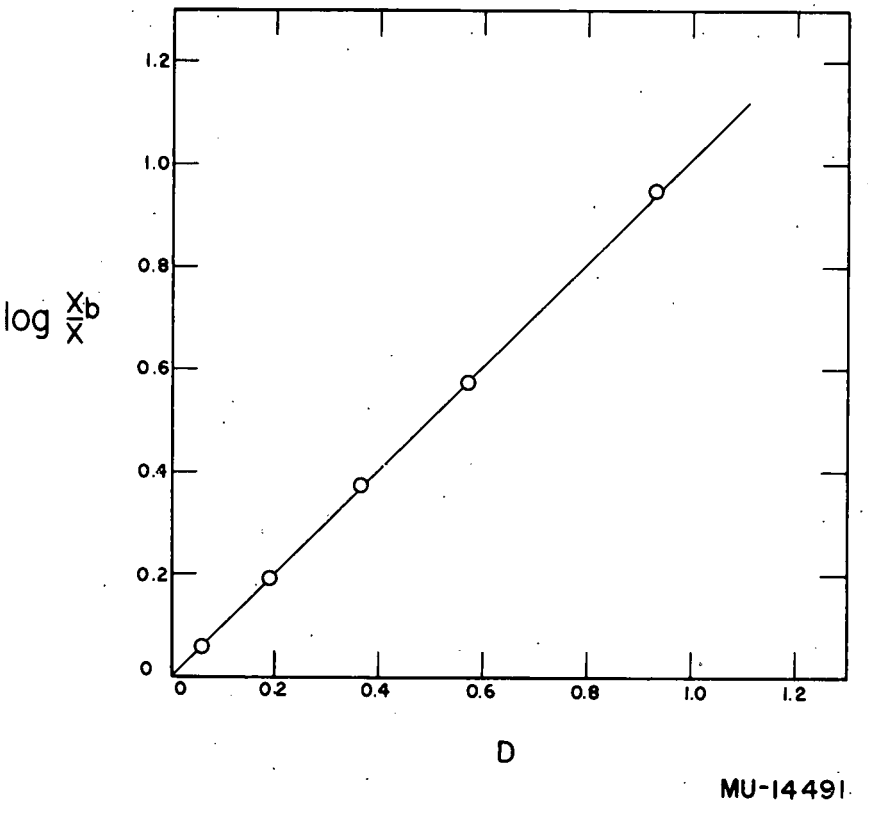

Fig. 3. Linearity of the oscilloscope with optical density.

used were brought beforehand to the expected temperature of the solution to minimize the error from heat exchange. His temperature-dependence data showed greater scattering than would have been predicted by non-systematic experimental errors. This was believed to be due to thermal effects from the walls, i.e., high-temperature runs would be slower than expected, owing to some cooler solution at the walls, and low-temperature runs in a similar way would be faster than expected.

A check on this method for measuring the temperature was made by placing a thermometer inside the mixer and comparing temperatures inside with temperatures of withdrawn samples. The comparison showed inconsistencies of a degree or more, and as much as a half degree warming even at room temperature.

Since it was difficult to thermostat the mixing device, because of its size, the filling operation, and the firing procedure, it was concluded that the most promising method would be to measure temperatures directly inside the mixer. This was done by inserting a Western Electric 14B thermistor into the mixing chamber. The leads were coated with Tygon paint to avoid shorting out the circuit and also to avoid reaction with the solutions. The resistance was measured with a Leeds and Northrup Wheatstone bridge, which permitted temperature measurement to $\pm$ 0.02°. The thermistor was previously calibrated in a Dewar system with a thermometer calibrated by the National Bureau of Standards. A plot of log R (R is resistance in ohms) versus $1000/T^{\circ}K$ gave excellent straight lines. The thermistor has been found to be stable and reproducible to this accuracy after at least one year's usage.

Calculations on Mixing Phenomena

Mixing

The mixing apparatus as developed by Below had been used to follow the rates of reactions with half lives of a few tenths of a second down to a few hundredths of a second. No attempt had been made to develop a model for mixing that might tell whether or not this apparatus was operating at an optimum limit of performance or whether it might with modifications be extended to the study of even faster reactions.

The only feasible test of the validity of such a model is to compare values of the time for a certain percentage mixing and the total amount of energy put into the system, since these are the only quantities directly observable. It was therefore necessary to set up a model for which one could derive equations relating these quantities and then to evaluate the validity of the model by comparing calculated values with those experimentally observed.

As a working model for mixing it was assumed that the work exerted on the liquid reactants by the spring system and transmitted to the liquids by the turbulator plate and baffle movement acts to break the liquids into small "cells." These "cells" then attain molecular mixing by diffusion.

The simplest diffusion case applicable to the system under consideration is that of unidimensional diffusion in a finite system. This is shown diagrammatically by the representation below, in which A and B represent the cross sections of two adjacent "cells," containing initially two different reactants.

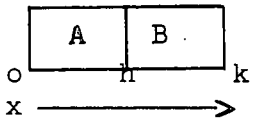

Starting from the general diffusion equation:

$$\frac{\partial C}{\partial t} = D \frac{\partial^2 C}{\partial x^2} ,$$

where C is concentration, t is time, and D is the diffusion coefficient, one can obtain a general solution for diffusion within parallel boundaries:

$$C = \frac{2}{k} \sum_{n=1}^{\infty} e^{-(n\pi/k)^2 Dt} \sin \frac{n\pi x}{k} \int_0^k f(x') \sin \frac{n\pi x'}{k} \, dx' .$$

Conditions for the above solution are: D may not be a function of C, and at $t = 0$, $C = f(x')$ for $0 \leq x \leq k$; also $\frac{\partial C}{\partial x} = 0$ at $x = 0$ and at $x = k$ for all values of t. The solution may be further simplified by defining

$$f(x') = C_o \text{ for } 0 < x < h ,$$

$$f(x') = 0 \text{ for } h < x < k \text{ and for } k > h.$$

The solution for this particular case is

$$C = C_o \left(\frac{h}{k} + \frac{2}{\pi} \sum_{1}^{\infty} \frac{1}{n} e^{-(n\pi/k)^2 Dt} \cos \frac{n\pi x}{k} \sin \frac{n\pi h}{k} \right) . \qquad (1)$$

Eq. (1) would give the concentration or percent mixing at a specific distance x. A more meaningful value would be the average concentration or the percent mixing throughout the "cell" area. To obtain the average concentration it is necessary to integrate Eq. (1) over the "cell", giving,

$$\frac{1}{h} \int_0^h C \, dx = C_o \left[\frac{h}{k} + \frac{2k}{\pi^2 h} \sum_{1}^{\infty} \left(\frac{1}{n} \right)^2 \exp -(n\pi/k)^2 Dt \left(\sin \frac{n\pi h}{k} \right)^2 \right]$$

Dividing by C_o, letting 2h = k, and simplifying, one obtains

$$\frac{\frac{1}{h}\int_o^h C\,dx}{C_o} = 0.50 + \frac{4}{\pi^2}\sum_o^{\infty}\frac{1}{(2m+1)^2}\exp\left[\frac{-\pi^2 Dt}{k^2}(2m+1)^2\right], \quad (2)$$

where the term on the left side of Eq. (2) is the average fraction of a species remaining in its original "cell." Representing the summation term by S, one may now define percent mixing

$$\% \text{ Mixing} = (0.50 - 0.405\ S)2\text{x}10^2. \quad (3)$$

The factor of 2 is necessary to account for diffusion from both cells A and B.

The percent mixing values in column 4 of Table I were obtained by using Eqs. (2) and (3) and selecting various values of k, t, and D.

Table I

Calculated percent mixing values ($D = 10^{-5}$ $cm^2/sec.$)

k x 10^4 cm	t x 10^3 sec	S	% Mixing
1	1	0.000	100
2	1	0.086	93
2.2	1	0.130	89
2.5	1	0.210	83
3	1	0.336	73
10	1	0.955	23
$10^{1.5}$	1	1.144	7
7	10	0.130	89
8.1	13.5	0.130	89
10	16	0.210	83
11.3	32	0.086	93

It is now necessary to obtain an equation that will relate the sizes of the "cells" to the amount of work necessary to break a body of liquid into such "cells." Since only unidimensional diffusion was considered, the analogous shearing model for the bulk liquid would be to split it into thin layers and interleave them, as shown diagrammatically below, where d_x, d_y, and d_z are dimensions of the bulk liquid and x is the thickness of a single layer.

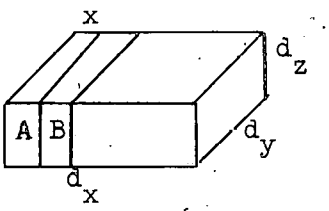

For laminar flow the force necessary to shear a liquid into such layers is

$$-F = \eta S \frac{dv}{dx} , \qquad (4)$$

where F is the force, η the viscosity of the fluid, S the total surface area sheared, and dv/dx the velocity gradient in the direction perpendicular to the plane of shearing. No attempt has been made to handle this problem by considering turbulent-flow models, and the system is almost certainly turbulent. However, such a model would require much more information about the flow properties in the mixing apparatus, and these data were not available. Turbulent flow in general involves a decrease in mass transfer along the direction of flow; that is, more of the kinetic energy is involved in motion transverse to the direction of flow. Because the shearing models are idealized, the mixing calculations should yield a minimum value for the energy required for mixing. Any turbulence would tend to increase the energy input necessary to impart the same flow characteristics, and would therefore seem to lead to a greater energy

requirement. However, this transferse motion due to turbulence is not necessarily inefficient in the mixing process, therefore the calculations based on laminar flow models may not be quite so faulty as was first believed.

The kinetic energy of the moving liquids is $E = 1/2\ MV^2$, and since V varies throughout the layers, one has

$$E = \frac{1}{x_0} \int_0^{x_0} \frac{1}{2}\ MV^2\ dx\ ,$$

where x_0 is the thickness of a single layer. For a single layer moving relative to two bounding layers the velocity decreases linearly from the center of the moving layer to the two layer boundaries, and the above equation can be rewritten

$$E = \frac{2}{x_0} \int_0^{x_0/2} \frac{1}{2}\ M\ (V_m \frac{2x}{x_0})^2\ dx\ ,$$

where V_m is the velocity at the center of the moving layer. This equation, on integration, gives

$$E = \frac{1}{6}\ MV_m^2 \quad \text{or} \quad dE = \frac{1}{3}\ MV_m\ dV_m . \tag{5}$$

From Eq. (4) one obtains

$$-\ dE = \eta S \frac{dV}{dx}\ d\ell\ ,$$

where ℓ is the distance necessary to move the sheared layers, and for this particular case we have $\frac{dV}{dx} = \frac{2V_m}{x_0}$, giving

$$-\ dE = \frac{2\eta S V_m}{x_0}\ d\ell\ .$$

Assuming that the kinetic energy of the liquids is used entirely in the

shearing process, the above equation and the differential form of Eq. (5) give

$$V_m - V_m^0 = \frac{-6\eta S\ell}{Mx_0} ,$$

where V_m^0 is the initial velocity. Since $\frac{d\ell}{dt} = V_m$, then

$$\frac{d\ell}{dt} = V_m^0 - \frac{6\eta S\ell}{Mx_0}$$

and

$$t = \frac{-Mx_0}{6\eta S} \ln \left(1 - \frac{6\eta S\ell}{V_m^0 Mx_0}\right) .$$

Solving for V_m^0 gives

$$V_m^0 = \frac{6\eta S\ell}{Mx_0} \left(\frac{1}{1 - \exp. \frac{-6\eta St}{Mx_0}} \right) ,$$

and, on substitution into Eq. (5),

$$E^0 = \frac{6(\eta S\ell)^2}{Mx_0^2} \left(\frac{1}{1 - \exp. \frac{-6\eta St}{Mx_0}} \right)^2 , \qquad (6)$$

Equation (6) can now be used to calculate the energy put into the shearing process.

The value of ℓ in Eq. (6) warrants some discussion. It is essentially the distance that one must move sheared layers of one reactant to obtain an alternating arrangement of these layers with those of the other reactant. For the purpose of the present calculation, in which we are attempting to obtain a minimum estimate of the energy required for mixing, it is assumed that the shearing takes place only along that direction which is most efficient. This implies that ℓ is related to the minimum geometrical

dimension of the bulk liquid, and in the case of a single-plate baffle it would be approximately equal to 1/2 the minimum over-all dimension. In the baffle used by Below (Fig. 1) one sees that ℓ would be 1/18 of the distance perpendicular to the laminae, or approximately 1/18 of the light-path distance. In the baffle being used presently (Fig. 2) ℓ would be 1/4 of the distance d_y.

In Eq. (6) x_0 has been defined as the thickness of a single layer. With respect to the diffusion model developed earlier, x_0 is then equal to k. At first thought one might equate x_0 with h or 1/2 k; however, this would not allow for diffusion in both the +x and -x directions, which most probably does occur to a great extent, since the "cells" of one reactant are in general located between "cells" of the other reactant.

From the assumed model one can now calculate the amount of energy E_0 necessary to give the experimentally observed mixing times and mixing ratios. This energy can then be compared with the actual energy put into the system.

Below reported 90% mixing in 12 to 15 milliseconds. His values are based primarily on a single experiment in which the neutralization of 0.01 M sodium p-nitrophenolate by 0.01 M perchloric acid was followed in the mixing apparatus. As seen in Table I, this mixing time gives a value of k of about 8×10^{-4} cm. From the actual dimensions of the mixer, d_x = 5.4 cm, d_z = 3.75 cm, and d_y = 1.45 cm; from the viscosity of water at 25°C (0.8937 centipoises); and from the mass of aqueous solutions mixed (approximately 90 grams) Eq. (6) gives $E^0 = 3.0 \times 10^9$ ergs.

This energy for mixing must now be compared with the total energy input available to the mixing process. The average spring force of the

triggering system is 30 pounds, approximated from the known initial and final spring forces. Thus the total energy input is $E^t = 5.0 \times 10^7$ ergs. However, not all this energy is available for mixing, since some must be used in accelerating the baffle.

High-speed photographs of the mixer in the firing process indicate that the baffle requires about 1.5×10^{-2} second to rise its total distance of 3.75 cm. These photographs were taken with a Fastex 16-mm camera at about 4500 frames per second, using Cine-Kodak Tri-X Reversal film, and analyzed with a low-power microscope. The exact value of the time is uncertain because extrapolation below and above the window was necessary.

Using the above time and distance and assuming the acceleration to be constant, one obtains 1.65×10^7 ergs for the energy required to accelerate the baffle, which weighs 150 grams. This is approximately one-third of the total applied energy (E^t), and the remaining two-thirds is available for mixing and frictional losses.

The values of E^0 and $2/3\ E^t$ are obviously inconsistent, with E^0 roughly 100 times as great as the available applied energy. Although it appeared certain that the difference could be due only to the inadequacy of the model, the same calculation was made for the experimental results of this study.

The mixing times and ratios for the new baffle were again measured, by use of the same reaction as Below had used. Values obtained from three experiments indicate about 83% mixing in 16 milliseconds and 93% mixing in 32 milliseconds, which is somewhat slower than Below had observed. These values lead to a k of 1×10^{-3} cm (Table I). Repeating the calculation for E^0, one obtains a value of 1.8×10^9 ergs, which is only slightly smaller than that calculated from Below's results, and

still considerably larger than any reasonable value. In all calculations to follow, the results will be based on the mixing values obtained in this study.

Since a unidimensional shearing-diffusion model does not give reasonable results the next logical approach was to allow both diffusion and shearing to take place in all directions. Such a model was set up and it was seen that introducing additional directions for diffusion could not give the order-of-magnitude changes that are necessary to bring the calculated energy values into agreement with the available energy. However, indications were that changes in the shearing model could bring about very significant changes in the energy calculations.

For the revised model, let us consider a cube of unit volume, 1 cm on each edge, and assume that linear diffusion will mix "cells" that are 1×10^{-3} cm thick, in the desired time. The most obvious method for shearing this cube would be to cut in one direction with a series of planes 1×10^{-3} cm apart and then move these planes an average distance of 1/2 cm. From Eq. (6), the geometry-dependent part is $S\ell/x$, and for the above shearing process equals $\frac{1(1/10^{-3} - 1)}{10^{-3}} \frac{1}{2} = \frac{1}{2} \times 10^{6}$ cm^2. One could also obtain "cells" that are mixed and have a thickness of 1×10^{-3} cm by cutting first in the x direction a small number of times and moving the "cells" a distance of 1/2 cm, then cutting in the y direction a small number of times and moving the "cells" a shorter distance determined by the number of first cuts in the x direction, and finally cutting in the z direction the desired number of times (i.e., cuts 10^{-3} cm apart) but now moving the cells only a very short distance determined by the first two cuts. Such a process can essentially minimize the distance required to move "cells" and at the same time obtain "cells" of a certain required

thickness. A rough calculation using 80, 80, and 1000 cuts successively gave a value for $S\ell/x$ of 0.016×10^6, which means a decrease by a factor of 30 in this quantity.

To apply this selective shearing model to the experimental situation requires first a consideration of the geometrical properties of the bulk liquid and the baffle. In the baffle under consideration (shown in Fig. 2), the two reactants initially are separated, one inside B and the other surrounding B. When the baffle is fired it moves in the d_z direction 3.75 cm, thereby breaking the bulk liquid into three layers, the center one twice as thick as the two outer layers. It is seen that further shearing by xz planes at this stage would not contribute to mixing, whereas cutting with either xy or yz planes does lead to mixing, and the distance necessary to move the sheared layers is $d_y/4$. One can now apply Eq. (6) to this situation, giving

$$E^0 = \frac{6\eta^2}{M} \left\{ \left[d_y d_z (n_x - 1) \frac{d_y n_x}{4 d_x} \right]^2 + \left[d_x d_y (n_z - 1) \frac{d_x n_z}{n_x d_z} \right]^2 + \left[d_x d_z (n_y - 1) \frac{d_z n_y}{n_z d_y} \right]^2 \right\}, \tag{7}$$

where for simplication the exponential term has been neglected; it is shown later that this term actually is negligible under the conditions here used. In Eq. (7) n_x, n_y, and n_z are the numbers of shearing layers along the corresponding directions. The first term in the brackets represents $(S\ell/x)^2$ for cutting with yz planes, the second with xy planes, and the third with xz planes. Another solution would be obtained by interchanging the directions of the second and third cuts. As stated above, the first cut could also be made with xy planes, which would give two additional solutions, depending on the order of the remaining two cuts. The value of

n_y in Eq. (7), or the corresponding last-cut n value for the other three solutions, is determined by the diffusion distances calculated and shown in Table I. A minimum value of E_0 was obtained by taking partial derivatives of Eq. (7) with respect to n_x, and n_z, and substituting these back into Eq. (7), giving

$$E^{0m} = \frac{6\eta^2}{M}\left[d_x d_z d_y^{8/7}(n/d)^{8/7} \right]^2 \quad (1/4 + 1/2 + 1) . \qquad (8)$$

Each of the four possible solutions gave this same minimized result, indicating that the order of shearing with respect to geometry is immaterial for the minimum. The value of n/d is always for the last cut, and is therefore equal to 1/k from the diffusion calculations.

The values of d_x/n_x, d_z/n_z, and d_y/n_y were 14.4×10^{-3} cm, 2.8×10^{-3} cm, and 10^{-3} cm respectively when calculated for the minimized E^{0m} and on the assumption that d_y/n_y had to be 10^{-3} cm according to the unidirectional-diffusion results. From these values it is seen that the results from the unidirectional-diffusion model are applicable, since the "cells" are considerably flattened.

It can now be shown that the exponential term in Eq. (6) is negligible. By numerical evaluation of the exponents for the last cuts by the known values of d_x, d_y, and d_z, and the calculated values of n_z and n_y, values of -107 and -840 were obtained for the next-to-last and last cuts respectively. In these cases the entire term is therefore negligible. For the first cut the evaluated exponent was -4.0 and the entire term becomes $\left(\frac{1}{1-e^{-4.0}} \right)^2 = 1.04$. Therefore, this effect could only cause an increase in the calculated E^0 value of approximately 4%, and a change of this size can be neglected in the consideration of the over-all roughness

and simplicity of the model itself. At best the model can only indicate orders of magnitude, and these smaller uncertainties become insignificant.

Returning to Eq. (8) and calculating E^{Om} for 83% mixing in 16 milliseconds gives $E^{Om} = 2.0 \times 10^5$ ergs. This calculation has used the 1/x value for the unidirectional diffusion solution because of the earlier mentioned "cell" flattening. The resulting E^{Om} value is now much lower than the actual total applied energy of 5.0×10^7 ergs, and is therefore a theoretically possible result. The result is of course extremely idealized, and the actual energy required for shearing is probably much larger. Certainly in the turbulent-flow patterns the tendency would be to shear to the same extent in all directions, and such a highly ordered shearing as has been assumed here could not exist. However, the results do indicate the lower limit for a model from which one could expect to obtain the observed mixing results.

The foregoing discussion on ordered shearing considered only the case for one cut in each direction, i.e., a total of three cuts. It is possible to make the shearing even more efficient by allowing repeated cuts in the different directions. A precise solution for such a model was not carried out. However, it can be shown that the last cut made, irrespective of the order of the preceding cuts, requires the most energy. The amount of energy required to make the last cut could not be decreased below that of Eq. (8) by more than a factor of about four.

One could further attempt to check the validity of the mixing calculations by varying the spring force and repeating the calculations, using the newly observed mixing times. If the relationship between the calculated and observed values was similar to that in this study, one

might assume that the model is basically correct but that its efficiency has been overly simplified through the use of highly ordered shearing. It may be that at different spring forces entirely different comparisons would be obtained owing to the changing effect of the turbulence upon the shearing process. It seems possible that such a study would be fruitful and could give added information about the mixing phenomena. However, owing to time limitations, such a study has not been carried out in the work reported here.

Consideration of the diffusion-model calculation indicates another inherent fault besides the assumption of idealized shearing. In the calculation of values of k, actual mixing times were used and the resulting "cell" sizes correspond to a diffusion process over that length of time. These same time values were also used in calculating the energy required to create the "cells." Certainly actual mixing time values are too large in the calculation because the shearing is done throughout some finite time period and not all the "cells" will have this much time to diffuse. The fault is trivial for the situation being studied since the value of t appears only in the exponential term of Eq. (6) and this term was always negligible in the calculation of E_0, indicating that the kinetic energy is dissipated very rapidly in comparison with the times for diffusion.

Accepting the diffusion shearing model, even though it is over-simplified and has wide limits of uncertainty, it is of interest now to see what possibilities exist for predicting mixer improvement, by altering the applied spring force. From the data in Table I, one sees that for the same mixing percentage (83) and a mixing time of 1 millisecond instead of the value of 16 milliseconds observed experimentally, the calculated value of k would be 2.5×10^{-4} cm as compared with 10×10^{-4} cm. E^{Om} is

approximately proportional to $1/k^2$ (Eq. (8)), and increase in E^{Om} by a factor of about 16 would be necessary -- an increase that is clearly beyond any practical modifications of the apparatus. To just lower the mixing time to 10^{-2} second would require an increase in E^{Om} by a factor of about 1.5. This indicates that not much can be gained in the mixing times by moderate increase of the applied spring force, and that with the present baffle and turbulator plate the mixer may be operating at almost optimum conditions.

Some improvement might be made by reducing the size of the bulk liquid; however, this is very limited because (a) the long dimension (d_x in Fig. 2) represents the optical light path, and any decrease in it would decrease the accuracy of measurements at low concentrations, (b) the smaller dimensions could not be cut by more than a factor of two, owing to mechanical problems. These changes would give no large advantage in mixing characteristics.

The calculated E^{Om} values were only about 1% of the applied E^t value. If one assumes that the selective-shearing model does describe the actual system to some extent it becomes clear that a baffle system that takes the maximum advantage of the shearing model might achieve much faster mixing times. In principle the baffle used by Below approached this idea. A baffle that separates the reactants into alternate laminae before mixing is initiated tends to reduce the distance ℓ which one has to move sheared "cells" in order to mix them. Unfortunately, Below's laminae were cut along the longest mixer dimension, with the result that the distance necessary to move "cells" was almost as great as that for the second baffle.

Bubble Formation

Below had observed that if solutions were not outgassed before being put into the mixing apparatus, severe bubble formation was observed when the mixer was fired. This did not occur when the solutions were previously outgassed under moderate vacuum (about 3 cm Hg) and drawn into the evacuated mixer.

It was of interest to investigate this somewhat further in order to understand the mechanism of bubble formation and possibly eliminate the necessity of outgassing by proper modification. It would be desirable to eliminate the outgassing process, both for convenience of experimental work and also to enable one to study reactions which require dissolved gases in the reactants or which require the presence of a volatile solvent.

Bubble formation can probably arise from at least four different causes: (a) The turbulent motion of the liquids may swirl air into the solutions: this could be either air above the liquid level or bubbles trapped beneath the liquid level. (b) Nucleation of dissolved gases may occur in the liquids due to a sudden lowering of pressure as the baffle is raised rapidly. This is similar to the formation of bubbles in solutions to which a vacuum has been applied. (c) Cavitation may occur and dissolved gases may diffuse to the low-pressure region, leaving bubbles when the cavity collapses after the baffle ceases to rise. (d) Water may evaporate into the cavity, taking with it any dissolved gases.

The first approach was to attempt a calculation to see whether or not the diffusion of dissolved gases could conceivably deposit enough gas in a cavity to cause serious bubble formation. The problem was treated as diffusion in a semi-infinite system, that is, one in which it is considered that the liquid body is essentially infinite at one end and

has a liquid-gas interface at the other end. It was assumed that the transfer of gas across the interface was very much more rapid than the rate of diffusion in the liquid body, therefore one can assume zero gas concentration at the interface at all times. The solution of the general diffusion equation for such a system is

$$C = \frac{2C_o}{\sqrt{\pi}} \int_o^{x\eta} e^{-B^2} \, dB \ ,$$

where C = concentration of diffusing substance,

C_o = initial concentration,

x = distance along diffusion path,

$\eta = 1/2 \sqrt{Dt}$,

D = diffusion coefficient,

t = time of diffusion;

then one has

$$C_o - C = C_o - C_o \phi (x\eta),$$

where

$$\phi(x\eta) = \frac{2}{\sqrt{\pi}} \int_o^{x\eta} e^{-B^2} \, dB$$

and Q, the quantity of gas that has diffused out of the liquid, is

$$Q = \int_o^{\infty} (C_o - C)dx = C_o \int_o^{\infty} \left[1 - \phi(x\eta) \right] dx \ . \qquad (9)$$

A plot of $\phi(x\eta)$ versus x, from Ingersoll, Zobel, and Ingersoll's values for $\phi(x\eta)$,[2] is shown in Fig. 4. From Eq. (9) it is seen that we have

$$Q = C_o A/\eta,$$

where A is the area between the curve and the line $\phi(x\eta) = 1$. It is

necessary to divide by η because the integration was actually carried out over ηdx and, according to Eq. (9), should be carried out only over dx. Measuring area A graphically and substituting $\eta = 1/2\sqrt{Dt}$, one obtains

$$Q = 1.12\ C_o \sqrt{Dt}.$$

Calculating C_o for nitrogen and oxygen from Henry's law, one obtains a total C_o of 8.0×10^{-4} $\underline{M}^*$. Using this and an average diffusion coefficient for oxygen and nitrogen in dilute solution of 2×10^{-5} cm^2/sec one obtains

$$Q = 4.0 \times 10^{-9} \sqrt{t}\ \text{mole/cm}^2 .$$

The results of the high-speed photographic studies on the mixer and also of a spectrophotometric study of the firing time indicate that the baffle is in motion for approximately 16 milliseconds. The area of the turbulator plate on the base of the baffle is 7.5 cm^2. Using these values and assuming that the cavity covers the entire turbulator plate and lasts throughout the baffle's motion, one obtains a total amount of 3.8×10^{-9} mole of gas diffusing into the cavity.

In addition to the diffusion of gas into the cavity, the vaporization of water into the cavity will also leave gas in this region. If one assumes that the pressure in the cavity is the vapor pressure of water at about 25°C, one calculates, using the ideal gas law, that approximately 2.3×10^{-5} cm^3 of water vaporizes into each cm^3 of cavity. Using the solubility of oxygen and nitrogen calculated earlier, one obtains 1.8×10^{-11} mole/cm^3 for the amount of gas deposited in the cavity by evaporation

---

*$\underline{M}$ will always herein represent concentration in moles/liter.

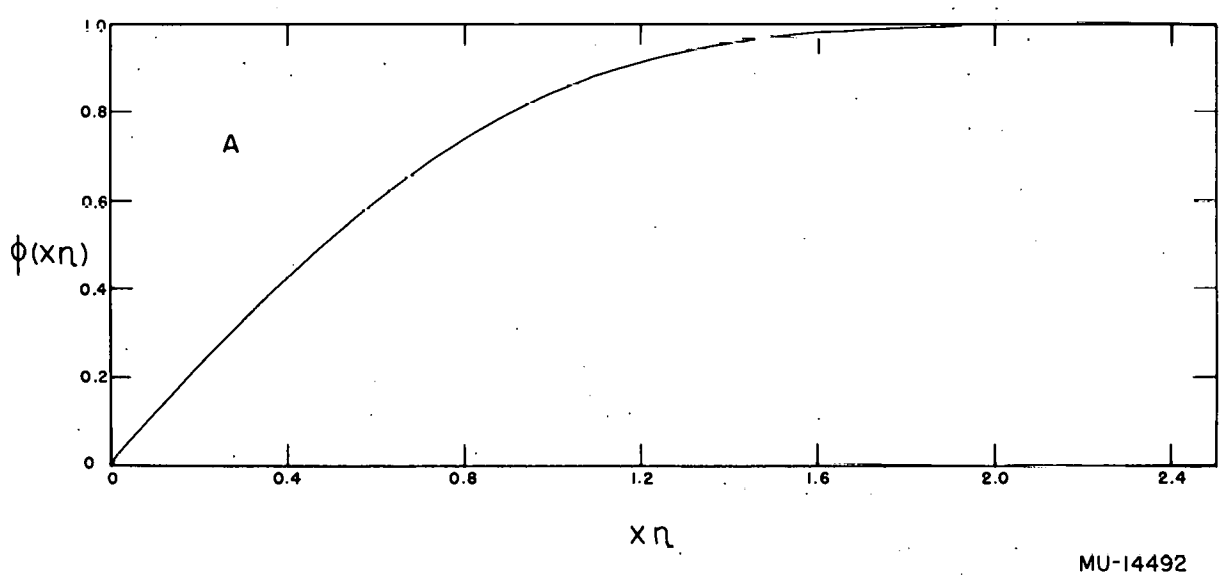

Fig. 4. Plot of $\phi(x\eta)$ versus $x\eta$.

of water. If one compares this amount with that obtained by the diffusion process it is seen that the vaporization contribution is completely negligible unless the volume of the cavity is of the order of 10 cm^3, and even then it amounts to less than 10% of the total gas in the cavity. It seems doubtful that the cavity can be of this order of magnitude in size, and therefore one may neglect the vaporization effect.

There is an alternate approach to the diffusion-cavity solution. This takes advantage of the concept of accommodation coefficients as discussed by Emmert and Pigford.[3] Here one postulates that there is not thermodynamic equilibrium at the gas-liquid interface and that only a fraction of the gas molecules striking the surface penetrate it. This may be thought of as involving some type of activated species in the interface so that a certain activation energy is required to cross this barrier.

The number of moles striking the surface from the cavity side per unit area per unit time is

$$R_g = \frac{1}{6} C_g \bar{v} ,$$

where C_g is the concentration of gaseous species and $\bar{v}$ is their average velocity. From kinetic theory of gases, one has

$$\bar{v} = \sqrt{\frac{8RT}{\pi \text{ mol.wt.}}}$$

The rate at which material enters the surface is then defined as

$$R_s = \frac{1}{6} C_g \bar{v} a ,$$

where a is the accommodation coefficient. The rate at which the dissolved gas evaporates from the liquid is defined as R_l, and it is seen

that it is

$$R_1 = k_1 C_1 ,$$

where k_1 is a rate constant and C_1 is the concentration of dissolved gas. It will be assumed in this case that C_1 is essentially constant owing to turbulence in the liquid. It is this assumption that C_1 is constant which indicates that this type of solution is more reasonable than the earlier calculated diffusion case, since it seems very likely that the vigorous motion of the liquids will tend to eliminate any concentration gradients. At equilibrium the rates of solution and evaporation of gas will be equal, therefore one obtains

$$R_1 = \frac{1}{6} C_g' \sqrt{\frac{8RT}{\pi \text{ mol.wt.}}} \quad a,$$

where C_g' is the concentration of air in the gas phase at equilibrium, i.e., 1 atmos. Using Emmert's and Pigford's value for oxygen, (4×10^{-8}),[3] one can now calculate R_1. Assuming that the pressure is 1 atmosphere after the baffle stops, C_g at 25°C equals 273/22,400 x 298 moles/cm^3. The molecular weight used was 28.8 grams, which is a weighted mean for oxygen and nitrogen in their proper ratios. These values gave R_1 as 1.3×10^{-8} moles/cm^{2}sec, which for 16 milliseconds and a cavity area of 7.5 cm^2 gives the amount of gas transferred into the cavity as 1.5×10^{-9} moles. This is to be compared with the value of 3.8×10^{-9} moles calculated from the diffusion model.

As was stated earlier, the accommodation-coefficient calculation was believed to be more valid; it is now also seen that this calculation leads to the slower rate of the two possible mechanisms and would in any case be rate-determining. It is doubtful that the numerical difference

between these two models is of any importance for the purpose of the present investigation; this becomes more obvious after calculation of the volume of bubble space which these amounts of gas are capable of forming. Assuming the pressure after the collapse of the cavity is 1 atmosphere, one obtains for the diffusion result (3.8×10^{-9} moles) a volume of 9.4×10^{-5} cm^3 of gas at 25°C, which would only give one bubble with a radius of 2.8×10^{-2} cm or numerous smaller bubbles. However, the bubble formation observed is very much larger than this. A rough estimate, based on visual observation, would indicate the total bubble volume to be in the 1-cm^3 region. This would require an increased factor of about 10^4 in some parameter in the equations for the diffusion results, and a slightly larger factor for the accommodation-coefficients results. It is doubtful that any quantities except possibly the cavity area are wrong by more than a factor of 2. The cavity area in contact with liquid may be greatly increased owing to swirling of the liquid, and it is the extreme of such a situation -- that is, no large cavity but many nucleations throughout the liquid body -- which will be mentioned next. It seems reasonable from the preceding calculations to rule out the large-cavity mechanism for bubble formation. This is somewhat further substantiated by the results of the high-speed photography of the mixer in the firing process. No cavitation was observed in films running at 4500 frames per second, and it seems reasonable to assume that a cavity that collapses this rapidly, if it exists at all, cannot be the cause of bubble formation.

The remaining possible mechanism for bubble formation arising from dissolved gases is that of nucleation at a great number of sites

in the liquid body, the nucleation being initiated by a reduced pressure due to the baffle's rapid removal.

No previous work on this type of problem was found. Earlier work had been done by Knapp[4] and Plesset[5] on the cavitation mechanism of vapor-bubble formation, in which it was shown that for certain turbulent-flow systems vapor bubbles formed and collapsed very rapidly, in approximately 2 milliseconds. These obviously could not be the cause of our bubble phenomena, which last for several seconds. They make no mention of observing bubbles with such long lifetimes, and yet their work was at more favorable conditions for cavitation than the work reported here.

One can treat this problem from a consideration of accommodation coefficients in a way similar to the cavity mechanism. Now one must let the bubbles grow from zero size, throughout the bulk liquid. Such a solution was attempted and the results indicate that in a time of 16 milliseconds (lifetime of the nucleation process) approximately 10^{11} very small bubbles would have to form and coalesce very rapidly. This calculation neglected the contribution of water vaporization to the bubble growth. Although the vaporization of water cannot contribute appreciably to long-lifetime bubbles by depositing dissolved air in the cavity, as was shown earlier, it is possible that this added growth during the formation period can appreciably increase the surface area available for air from the bulk liquid entering the cavity. Calculations on this effect showed that for it to be appreciable a very large gas volume would have to exist throughout the formation period. The high-speed photography results do not show any evidence for such large gas volume. Therefore, it seems questionable that such a nucleation process

can occur under the conditions here imposed.

The preceding discussion implies that neither a large cavity nor homogeneous nucleation could easily explain the observed bubble formation. This work led the author to believe that some cause other than dissolved gases must be the source of the bubble formation. In considering under what conditions bubbles were observed it was noted that there always existed a possibility of trapping air pockets on the mixer surfaces, either on the walls or under the baffle. When nonoutgassed solutions were drawn into the mixer under vacuum, outgassing occurred, probably leaving bubbles on the walls. It is possible that these bubbles formed in the filling process are later swirled into the mixing solutions. To check on the possibility of such surface effects two types of experiments were carried out. First, outgassed solutions were put into the dried mixer by gravitational flow; the mixer was at 1 atmosphere pressure. When the mixer was fired, extreme bubble formation was observed. This clearly indicates that surface effects are very important, and the next step was to attempt the elimination of such effects. The mixer was filled under vacuum with previously outgassed solutions -- the normal filling operation used in all kinetic studies. This method of filling is known to eliminate bubble formation. Once the mixer was filled, water saturated with air was forced in at the bottom of the mixer, displacing the outgassed water, which was taken out at the top of the mixer. This was done carefully so as to allow no bubbles to enter the mixer. The process was continued until several times the volume of the mixer had been removed at the top. The water inside the mixer was now certainly at equilibrium with 1 atmosphere of air. When the mixer was fired no bubble formation was observed, thereby clearly indicating that bubble formation is not due to dissolved gasses but probably to pockets

of air trapped on the mixer surfaces. Although this result now makes the preceding calculations reasonable, it does not immediately show a new method for avoiding bubble formation. The filling process described in the experiment above is not practical, and in actual kinetic runs it seems probable that vacuum filling with outgassed solutions will continue to be used. It may be possible to coat or polish the walls in such a way as to eliminate the bubble trapping, although at the present time no such method is known.

Orifice-Flow Limitation

One other aspect of mixer limitation should be considered, that is, the rate of flow through the turbulator plate. No matter how efficient turbulence is in mixing the solutions, the mixing time is always limited by the time required for these solutions to fill the observation chamber.

Using the equation for flow through circular orifices, one has

$$q = CYS \sqrt{\frac{2g\Delta H}{1-B^4}} ,$$

where q = volumetric rate of discharge,

C = coefficient of discharge (0.61),

Y = expansion factor (1 for liquids),

S = orifice area,

g = gravitational acceleration constant,

ΔH = pressure differential between upstream and orifice,

B^2 = ratio of orifice area to upstream channel area;

therefore

$$q = 0.61\ S \sqrt{\frac{1960\ \Delta H}{1 - B^4}} .$$

The channel area is approximately 7.8 cm^2 and the volume of liquid mixed below the turbulator plate is 29.4 cm^3. If the pressure differential is about 2 atmospheres (due to the compression of air above the liquids by the rising baffle -- the average spring force is about 30 pounds), then for the mixing to take place in 10^{-3} seconds, S (the orifice area) would have to be 7.4 cm^2, which is about 95% of the total turbulator-plate area. This is clearly impractical to construct and certainly would not provide adequate turbulence for rapid mixing.

Assuming that the maximum orifice area in an efficient turbulent plate is no more than 50% of the total area, then one can calculate the time required to fill the mixing chamber from the relationship $t = v/q$, where v is the volume of the mixing chamber and q is the volumetric rate of discharge. The resulting value for t is 7.5×10^{-3} second.

It becomes clear that this mixing apparatus is limited to mixing times somewhat below 10^{-2} second. In consideration of the results of the earlier mixing calculations, in which it was concluded that possibly only a very small part of the energy put into the system was required to do the mixing, it seemed plausible that a turbulator plate and baffle of different design might give much faster mixing. However, in consideration now of the limitations due to orifice flow, also, it seems that the increase in mixing could not be better than by a factor of two or three. It is doubtful that this possible gain warrants the work involved in designing a more efficient turbulator and baffle.

Part II

HEATS AND ENTROPIES OF ACTIVATION OF THE FERRIC THIOCYANATE REACTION

Introduction

Below has studied the kinetics of the formation of the first ferric thiocyanate complex in aqueous solution[1] and found the forward rate law to be

$$\frac{d(FeSCN^{+2})}{dt} = k_1(Fe^{+3})(SCN^-) + k_2\frac{(Fe^{+3})(SCN^-)}{(H^+)} .$$

At 25°C and at an ionic strength of 0.40 he obtained

$$k_1 = 124 \pm 10\ \underline{M}^{-1}\ sec^{-1},$$
$$k_2 = 21 \pm 2\ sec^{-1},$$
$$\Delta H_1^{\ddagger} = 10 \pm 1\ kcal/mole,$$
$$\Delta H_2^{\ddagger} = 24 \pm 3\ kcal/mole,$$
$$\Delta S_1^{\ddagger} = -15 \pm 8\ eu,$$
$$\Delta S_2^{\ddagger} = 27 \pm 12\ eu.$$

As was discussed in Part I, the temperature dependence results were questionable and the resulting entropies did not seem reasonable when compared with those for analogous reactions or with some equilibrium entropies of complexing. The purpose of this investigation was to re-measure the temperature dependence of this reaction with the modified apparatus.

Equilibrium Quotients

The principal equilibria between ferric and thiocyanate ions in solution are known to be

---

[1] $\ddagger$ will be used herein to designate heats and entropies of activation.

$$Fe^{+++} + SCN^{-} = FeSCN^{++} \qquad Q_{1s} = \frac{(FeSCN^{++})}{(Fe^{+++})(SCN^{-})} ,$$

$$FeSCN^{++} + SCN^{-} = Fe(SCN)_2^{+} \qquad Q_{2s} = \frac{(Fe(SCN)_2^{+})}{(FeSCN^{++})(SCN^{-})} ,$$

where parentheses indicate concentrations in moles per liter and Q is the value of the equilibrium quotient expressed in concentrations. Table II lists the thermodynamic values obtained by previous workers.

Table II

Thermodynamic Data for Ferric Thiocyanate Complexes

Reference	Method	Temp.	μ[a]	Q_{1s}	Q_{2s}	ΔH_{1s} (cal/mole)
Betts and Dainton[6]	Spectro-photometric	25.0°C	1.28	114	20	-1600
Frank and Oswalt[7]	Spectro-photometric	Room	0.5	138		
Laurence[8]	E.M.F.	25.0	0.5	139	20.5	-1500
Lister and Rivington[9]	Spectro-photometric	25.0	0.5	146	15.5	- 800

[a] Ionic strength

The work reported here was carried out at an ionic strength of 0.40. Below had determined the first complexing constant at this ionic strength to be $Q_{1s} = 146 \pm 5$ at 25°C. From Laurence's data and his ionic-strength correction equation,[8] Q_{1s} calculated is 149 at 25°C and $\mu = 0.40$. From

Lister's and Rivington's data and their ionic-strength dependence results,[9] Q_{ls} calculated is 144 at 25°C and $\mu = 0.40$. The final values chosen for the calculations of the kinetic runs were $Q_{ls} = 146$ (25°C, $\mu = 0.40$) and $\Delta H_{ls} = -1600$ cal/mole. The second complexing constant was not determined at $\mu = 0.40$ because experimental conditions were chosen to make its contribution negligible.

It was necessary to correct all data for the hydrolysis of ferric ion. Milburn and Vosburgh[10] found the principal equilibria to be

$$Fe^{+++} + H_2O = FeOH^{++} + H^+ \qquad Q_h = \frac{(FeOH^{++})(H^+)}{(Fe^{+++})} ,$$

$$2\ FeOH^{++} = Fe_2(OH)_2^{+4} \qquad Q_d = \frac{(Fe_2(OH)_2^{+4})}{(FeOH^{++})^2} .$$

From their data Q_h (25°C, $\mu = 0.40$) = 2.05×10^{-3} and $Q_d = 390$. The equilibrium quotients Q_h and Q_d were corrected for temperature by using ΔH values of 10.2 and -8.2[12] kcal/mole respectively,[11,12] measured for an ionic strength of 1.0.

Reagents

Distilled water was redistilled from alkaline permanganate. All chemicals were reagent grade.

Solutions of 0.1 M ferric perchlorate were prepared by dissolving spectroscopic grade iron rod in hot nitric acid, centrifuging to remove carbon, and then fuming with 72% perchloric acid. The resulting product, on addition of silver nitrate, showed by Tyndall beam about 10^{-5} M chloride ion. The solution gave no "brown ring" test for nitrate ion. Ferric ion concentration was determined by reduction with a Jones reductor column followed by titration with standardized ceric perchlorate

solution. Acidity was measured by the method of Schumb, Sherrill, and Sweetser,[13] i.e., a hot titration with sodium hydroxide to the phenolphthalein end point.

Sodium thiocyanate solutions were prepared from the recrystallized oven-dried salt and analyzed by silver nitrate titration. Reagent grade perchloric acid was standardized with sodium hydroxide, using potassium acid phthalate as primary standard. The sodium perchlorate solution used in adjusting the ionic strength was prepared by dissolving sodium carbonate in a slight excess of perchloric acid, heating to expel carbon dioxide, and titrating to neutrality with a small amount of sodium hydroxide. It was standardized by drying at 150°C and weighing as $NaClO_4$.

Rate Law

Below showed the rate law to be first-order dependent on both ferric and thiocyanate ion concentrations at constant hydrogen ion concentration. Writing the mechanism as

$$Fe^{+++} + SCN^- \underset{\bar{k}'}{\overset{\bar{k}}{\rightleftharpoons}} FeSCN^{++},$$

and using the relationship $Q_{ls} = \bar{k}/\bar{k}'$, one obtains

$$\frac{d(FeSCN^{++})}{dt} = \bar{k}\,(Fe^{+++})(SCN^-) - \frac{\bar{k}}{Q_{ls}}\,(FeSCN^{++}).$$

If (Fe^{+++}) is assumed to be essentially constant during an experiment, with (SCN^-) expressed in terms of $(FeSCN^{++})$, and if $(FeSCN^{++})_o$ and $(FeSCN^{++})_\infty$ are defined as the concentrations of complex at the start of the reaction and after attainment of the final equilibrium value, respectively, the above rate law may be integrated, yielding

$$-\bar{k}\,t = \frac{2.30}{(Fe^{+++}) + 1/Q_{ls}} \log \frac{(FeSCN^{++})_\infty - (FeSCN^{++})}{(FeSCN^{++})_\infty - (FeSCN^{++})_o} \quad . \qquad (10)$$

It is this equation which Below used and which is used in this work to determine values of $\bar{k}$, since all other quantities were determinable experimentally. The data for a typical experiment are given in Table III. Fig. 5 shows the negative for this experiment. The displacement on the negative of the trace from the dark current is equal to x. The value of 1.175 log x_b/x, where b signifies the blank, is equal to the optical density and therefore proportional to the $FeSCN^{++}$ concentration, since the experiments were run at a wave length (λ = 605 mμ) at which $FeSCN^{++}$ was essentially the only absorbing species. The numerical factor comes from the nonlinear characteristics of the first oscilloscope. The value of log x_b/x_∞ is similarly proportional to $(FeSCN^{++})_\infty$, the final $FeSCN^{++}$ concentration. Therefore log x_b/x_∞ - log x_b/x is proportional to $(FeSCN^{++})_{oo}$ - $(FeSCN^{++})$ and consequently the slope of a plot of the logarithm of the first quantity versus time yields $-\bar{k}\left[(Fe^{+++}) + 1/Q_{ls}\right]/2.30$. To solve for $\bar{k}$ the average ferric ion concentration was substituted for (Fe^{+++}).

Table III

Data for a typical experiment. Experiment 22 of Table IV and Figure 5

Temp = 23.38°C	$(HClO_4)$ = 0.224 M	$\Sigma(SCN^-)_{calc}=1.20\times10^{-3}$ M
μ = 0.40	$\Sigma(Fe(III))$ = 7.91×10^{-3} M	
Q_1 = 148	Final $(FeSCN^{++})$ = 6.16×10^{-4} M	$Av(Fe^{+++})_{calc}=7.51\times10^{-3}$ M

Time (sec)[a]	x[b] (mm)	log x - log x_∞
0.0	28.3	0.872
0.0'	28.5	0.864
0.05	23.7	0.795
0.05'	23.2	0.775
0.10	18.6	0.690
0.10'	18.5	0.677
0.15	15.2	0.602
0.15'	15.2	0.591
0.20	12.9	0.531
0.20'	12.8	0.517
0.25	11.3	0.474
0.25'	11.3	0.463
0.30	10.0	0.420
0.30'	10.0	0.409
0.35	8.9	0.370
0.35'	8.9	0.359
0.40	8.15	0.332
0.40'	8.2	0.323
∞	3.8	
∞ '	3.9	

[a] The primed entries are for the right side of the negative and the unprimed for the left.

[b] x of blank = 36.7

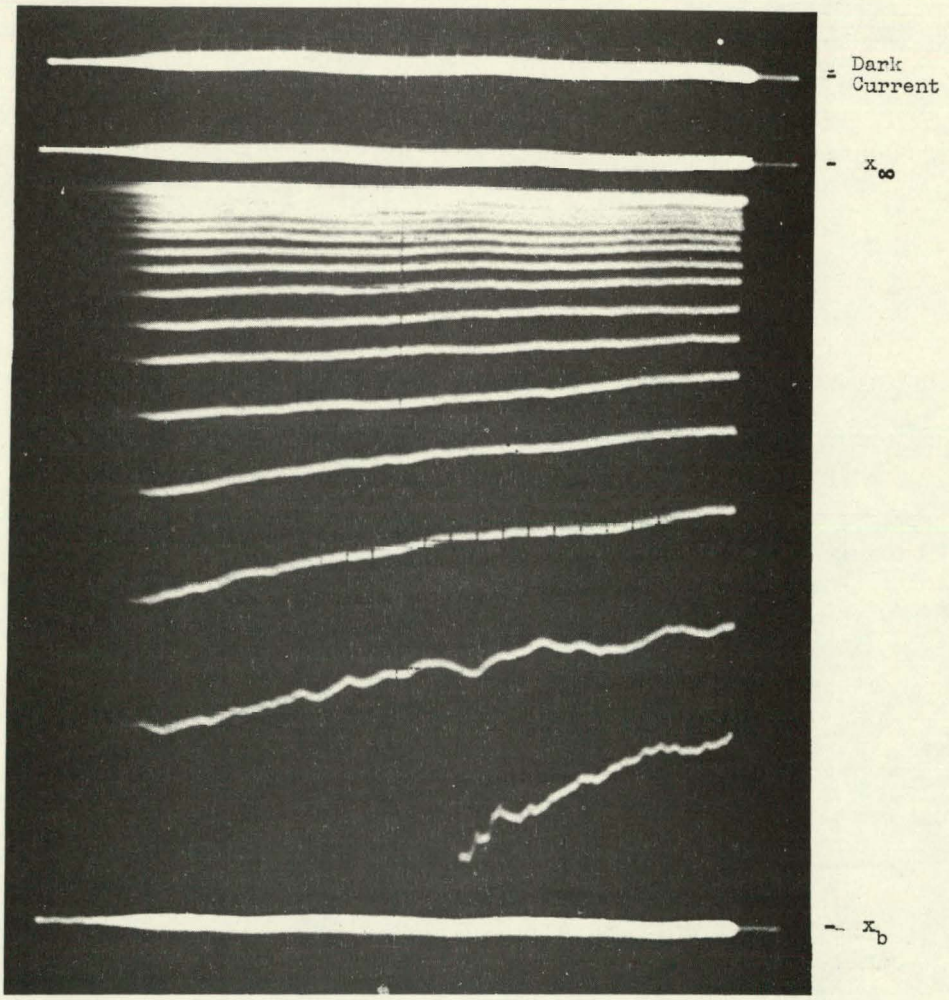

ZN-1848

Fig. 5. The negative of experiment III-18, Table III.

Calculation of $\bar{k}$ for a typical experiment

Figure 6 shows the semilogarithmic plot of log x - log x_∞ versus time for the experiment of Table III and Fig. 5. Since we have

$$\bar{k} = \frac{-2.30 \times \text{slope}}{(Fe^{+++}) + 1/Q_{ls}} , \qquad (11)$$

where the slope is that of the plot of log x - log x_∞ versus time, the only other quantity needed from experimental data is (Fe^{+++}). In general this could not be inferred from the concentrations of initial solutions because the mixing ratio of the two solutions was not usually 1:1. Therefore, at the conclusion of the run a 10-ml sample was removed from the mixer through the needle valves on the base plate and this solution was analyzed. The sample was first brought to room temperature, and its optical density measured at 610 mμ in a 2.00-cm cell on a Beckman DU spectrophotometer, thus giving the final concentration of $FeSCN^{++}$. Below had determined the molar extinction coefficient of $FeSCN^{++}$ at 610 mμ as a function of temperature to be

$$\epsilon_{610} = 271 + 7(t - 25) , \qquad (12)$$

where t is measured in degrees Centigrade.

A determination for Fe(III) was then made on the sample. Using the same method as Below: 1 ml of test solution was delivered into a 25-ml volumetric flask, 5.0 ml of 1.0 M perchloric acid was added to suppress hydrolysis, and the flask was filled to volume with 0.50 M sodium thiocyanate. The time was noted, a 1.00-cm quartz cell was filled and brought to 25 ± 0.5°C, and the absorption was measured at 610 mμ, the time of reading being noted. The inclusion of the time was necessitated by the slow decomposition of the complexes with time. The ferric ion was 98%

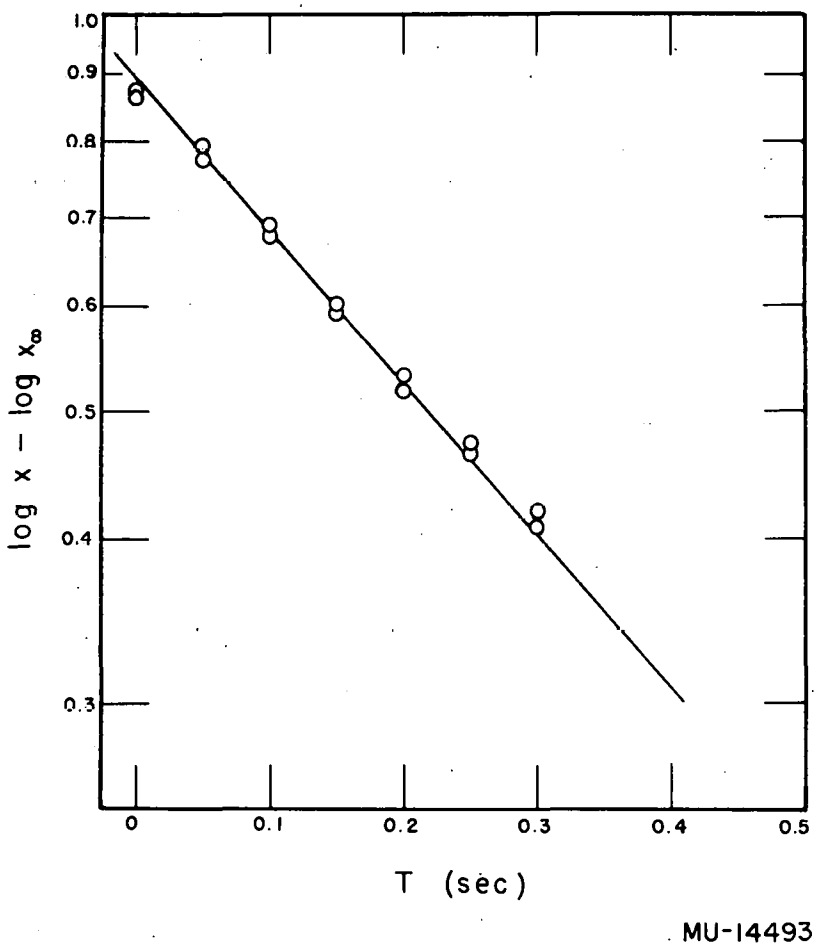

Fig. 6. The kinetic curve of experiment III-18, Table III.

complexed, and a check showed that ferric ion concentration was linear with optical density D. The result was obtained from the empirical equation

$$\Sigma \text{ Fe(III)} = 0.0185 \ (D + 0.0029t), \qquad (13)$$

t being the time in minutes elapsed between adding the thiocyanate solution to the test solution and making the absorption reading. It was generally on the order of 3 minutes.

As a check on the consistency of the analysis and in order to calculate the mixing ratio for the two solutions, the total initial thiocyanate concentration was calculated by two methods, following Below.

The mixing ratio method used the analysis for ΣFe(III). If $(Fe(III))_o$ is the stoichiometric concentration of ferric ion in the original solution to be mixed, and $(SCN^-)_o$ is the corresponding value in the original thiocyanate solution, then $\Sigma Fe(III)/(Fe(III))_o$ defines the dilution factor, α, for the iron solution. Therefore, the dilution for the thiocyanate is $1 - \alpha$, and

$$\Sigma \ SCN^- = (SCN^-)_o(1 - \alpha)$$

or

$$\Sigma \ SCN^- = (SCN^-)_o \left[1 - \frac{\Sigma \text{ Fe(III)}}{(Fe(III))_o}\right] . \qquad (14)$$

The equilibrium method used the values of ΣFe(III) and $(FeSCN^{++})_\infty$. From

$$Q_{1s} = \frac{(FeSCN^{++})_\infty}{(Fe^{+++})_\infty (SCN^-)_\infty}$$

one obtains

$$\Sigma SCN^- =$$

$$(FeSCN^{++})_\infty \left[1 + \frac{1}{Q_{ls}[(\Sigma Fe(III) - (FeSCN^{++})_\infty - (FeOH^{++})_\infty - 2(Fe_2(OH)_2^{+4})_\infty]} \right]. \quad (15)$$

The comparison of these two ΣSCN^- values generally agreed to better than 5% and the value of ΣSCN^- actually used was a mean of the two, weighted 2:1 in favor of the equilibrium value.

To obtain an average value of (Fe^{+++}) for use in Eq. (11), the average $FeSCN^{++}$ concentration is needed. This could not be obtained from the $(FeSCN^{++})_\infty$ alone because of some premixing, i.e.,

$$(FeSCN^{++})_{av} = \frac{(FeSCN^{++})_\infty + (FeSCN^{++})_o}{2},$$

and since

$$\frac{(FeSCN^{++})_o}{(FeSCN^{++})_\infty} = \frac{\log x_b/x_o}{\log x_b/x_\infty}$$

then

$$(FeSCN^{++})_{av} = (FeSCN^{++})_\infty \left[1/2 + 1/2 \frac{\log x_b/x_o}{\log x_b/x_\infty} \right], \quad (16)$$

with the $(FeSCN^{++})_\infty$ being known from the direct measurement following the run. In runs made at temperatures differing from the temperature of the later measurement of $(FeSCN^{++})_\infty$, a correction was made for the change of Q_{ls}. Now $(Fe^{+++})_{av}$ may be obtained from

$$(Fe^{+++})_{av} = \Sigma Fe(III) - (FeSCN^{++})_{av} - (\text{hydrolyzed Fe(III)})_{av}. \quad (17)$$

Proceeding now to calculate the experiment of Table III and Figs. 5 and 6: The two initial solutions contained 1.95×10^{-2} M ferric ion and 0.002 M thiocyanate ion respectively, and both had a hydrogen ion concentration of 0.224 M. After the run a sample in a 2.00-cm quartz cell at 610 mμ and a temperature of 25°C gave a net optical density of 0.334. A 1.00-ml sample of this test solution plus 5.0 ml of 1.0 M perchloric acid was diluted to 25 ml with 0.50 M sodium thiocyanate. The resulting solution gave a net optical density at 610 mμ in a 1.00-cm cell of 0.418, after an elapsed time of 3.31 minutes.

Using Eq. (12), one has $(FeSCN^{++})_{\infty,25} = 6.16 \times 10^{-4}$ M,

from Eq. (13), $\Sigma Fe(III) = 7.91 \times 10^{-3}$ M,

from Eq. (14), $\Sigma SCN^{-} = 1.19 \times 10^{-3}$ M,

at 25°C, $\mu = 0.40$, $Q_{ls} = 146$, $Q_h = 2.05 \times 10^{-3}$, and $Q_d = 390$. Using Q_h, Q_d, (H^+), $\Sigma Fe(III)$, and $(FeSCN^{++})_{\infty}$, one obtains

$$(FeOH^{++})_{\infty,25} = 6.62 \times 10^{-5} \text{ M},$$

$$(Fe_2(OH)_2^{+4})_{\infty,25} = 1.71 \times 10^{-6} \text{ M}.$$

From Eq. (15), $\Sigma SCN^{-} = 1.20 \times 10^{-3}$,

giving a value of $\Sigma SCN^{-}_{av} = 1.20 \times 10^{-3}$.

To calculate $(Fe^{+++})_{av}$ for the run that was at 23.38°C, one uses $Q_{ls} = 148$, $Q_h = 1.86 \times 10^{-3}$, $Q_d = 390$, $\Sigma Fe(III)$, ΣSCN^{-}, and (H^+), and obtains

$$(FeSCN^{++})_{\infty,23.38} = 6.20 \times 10^{-4},$$

$$(FeOH^{++})_{\infty,23.38} = 6.00 \times 10^{-5},$$

$$(Fe_2(OH)_2^{+4})_{\infty,23.38} = 1.41 \times 10^{-6},$$

and from Eqs. (16) and (17), $(Fe^{+++})_{av} = 7.50 \times 10^{-3}$. The slope in Fig. 6

is 1.16, therefore, from Eq. (11),

$$\bar{k}_{23.38} = \frac{(2.30)(1.16)}{7.50 \times 10^{-3} + 1/148} = 188\ \underline{M}^{-1}\ \text{sec}^{-1}.$$

It is clear that in this run the values of $(FeSCN^{++})_\infty$, $(FeOH^{++})_\infty$, and $(Fe_2(OH)_2^{+4})_\infty$ at 23.38°C did not need to be calculated. Considering the small correction that these terms make on $(Fe^{+++})_{av}$, the values calculated earlier for 25°C would have been accurate enough. This calculation was included only to indicate the procedure used in runs not close to 25°C, where the correction is somewhat larger.

Temperature-Dependence Runs

In order to determine the heats and entropies of activation a series of experiments was run covering the temperature range 13.7°C to 31.63°C and the $\bar{k}$ values obtained from these runs are shown in Table IV. The temperatures as measured by the thermistor are considered to be accurate to ± 0.05°. This is somewhat larger than the previously stated accuracy of thermistor measurements. The larger uncertainty is assigned because of small temperature differences in the solutions before mixing.

Considering the rate law determined by Below,

$$\frac{d(FeSCN^{++})}{dt} = k_1(Fe^{+++})(SCN^-) + k_2\frac{(Fe^{+++})(SCN^-)}{(H^+)}$$

it is apparent that $\bar{k}$ as defined and measured by Eq. (10) at constant (H^+) equals $k_1 + k_2/(H^+)$. Because of the two-term rate law, it was necessary to carry out temperature-dependence experiments at two different acidities. From the resulting data shown in Table IV a plot of log $\bar{k}/T^\circ K$ versus $1/T^\circ K$ was made for the two acidities (Fig. 7). Since the data showed no signs of specific curvature, the best-fitting straight

lines were drawn. The average deviation from these lines is approximately 5%. Values of $\bar{k}$ were taken from this plot at three temperatures corresponding to $1000/T^{\circ}K = 3.26$, 3.40, and 3.54, and from these were calculated values of k_1 and k_2 at these three temperatures.

Table IV

Temperature-dependence data

$\mu = 0.40$

Experiments 18-23: $(H^+) = 0.224$ M

Experiments 24-28: $(H^+) = 0.0308$ M

Experiment	Temperature ($^{\circ}C$)	(Fe^{+++}) (M x 10^3)	$\Sigma(SCN^-)$ (M x 10^3)	$\bar{k}$ (M^{-1} sec^{-1})
18	23.60	7.22	1.22	216
19	17.63	6.55	1.26	109
20	29.51	8.84	1.28	302
21	31.63	8.52	1.09	392
22	23.38	7.50	1.20	188
23	13.73	7.09	1.22	71
24	24.84	6.59	1.26	733
25	16.52	6.51	1.29	288
26	15.73	7.35	1.20	264
27	26.76	5.14	1.09	1053
28	30.15	8.21	1.47	1402

Fig. 8 shows a plot of $\log k_1/T^{\circ}K$ versus $1/T^{\circ}K$ and similarly for k_2. From the slopes of these lines, $\Delta H_1^{\ddagger} = 13.0 \pm 1.4$ kcal/mole and $\Delta H_2^{\ddagger} = 20.2 \pm 1.4$ kcal/mole were calculated. The corresponding entropies of activation at 25°C were calculated as $\Delta S_1^{\ddagger} = -5 \pm 5$ eu and $\Delta S_2^{\ddagger} = 15 \pm 5$ eu. The uncertainties were obtained by assuming a possible error of 10% in the rate constants at the high and low temperature.

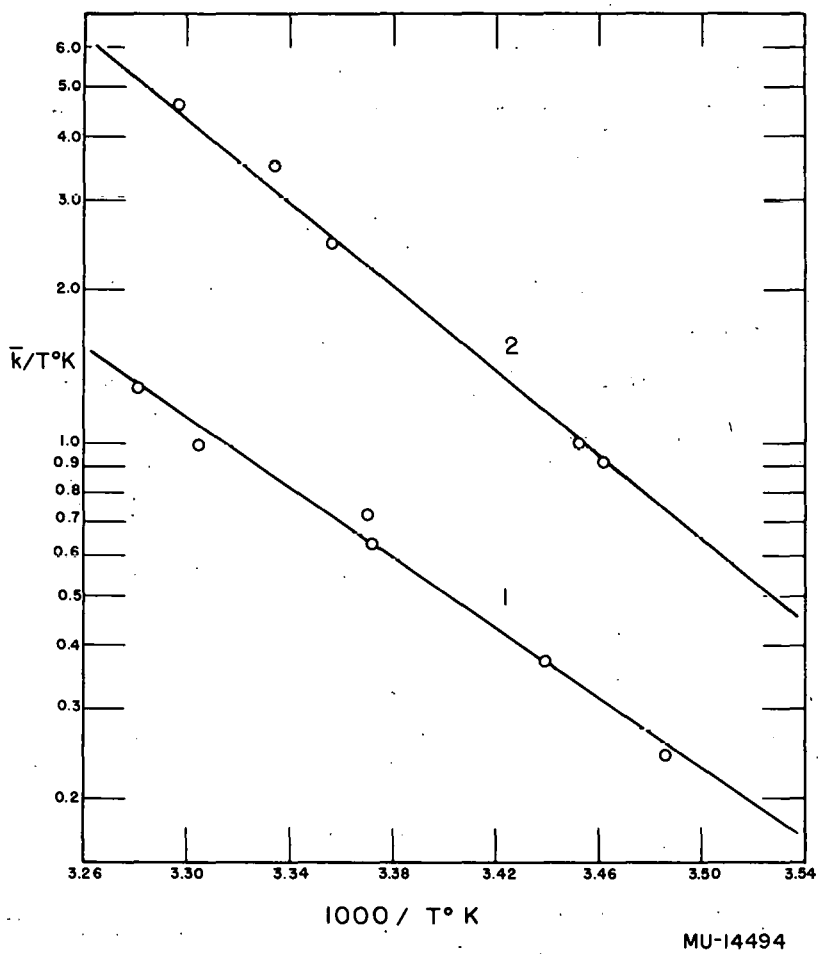

Fig. 7. The temperature dependence of $\bar{k}$. Curve 1: (H^+) = 0.224, Curve 2: (H^+) = 0.0308.

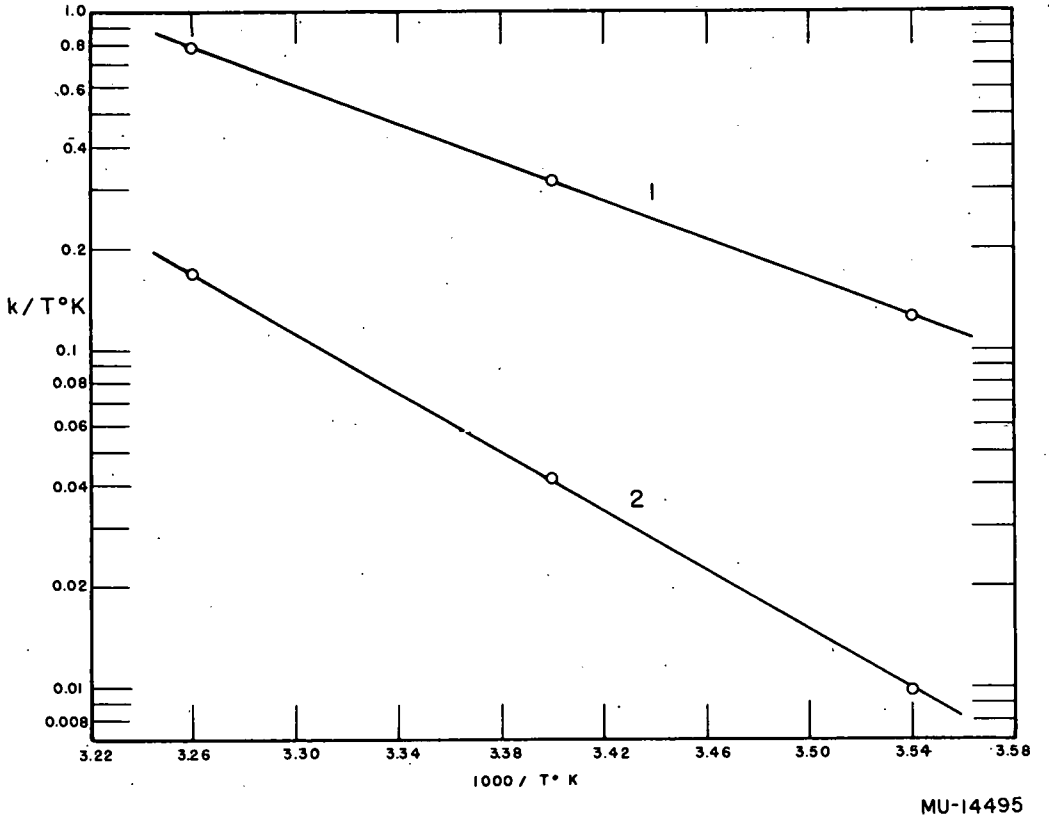

Fig. 8. The temperature dependence of k_1 (Curve 1), and k_2 (Curve 2).

Acid-Dependence Results

The above $\Delta H^{\ddagger}$ values and k_1 at 25°C were then used to correct Below's room-temperature $\bar{k}$ values to 25°C. These are listed in Table V. Also, $\bar{k}$ values at 25°C were obtained for the two acidities of this study, from Fig. 8. Figure 9 shows a plot of $\bar{k}$ at 25°C versus $1/(H^+)$. For $\bar{k} = k_1 + k_2/(H^+)$, such a plot should give a straight line with a finite intercept at $1/(H^+) = 0$, with the intercept being equal to k_1 and the slope being equal to k_2. The final values of k_1 and k_2 at 25°C were taken from this plot. They are $k_1 = 127 \pm 10$ $\underline{M}^{-1}$ sec^{-1} and $k_2 = 20.2 \pm 2$ sec^{-1}.

Table V

Kinetic data at room temperature. (μ = 0.40 unless otherwise noted)

Expt	Temp (^{o}C)	(Fe^{+++}) ($\underline{M} \times 10^{3}$)	$\Sigma(SCN^{-})$ ($\underline{M} \times 10^{3}$)	(H^{+}) ($\underline{M}$)	$\bar{k}$ ($\underline{M}^{-1}$ sec^{-1})	$\bar{k}_{25^{o}}$ ($\underline{M}^{-1}$ sec^{-1})
1	22.5	7.2	1.19	0.200	180	226
2[a]	23.2	6.8	1.29	"	209	249
3[b]	24.7	7.0	1.24	"	235	242
4[c]	25.5	(5.5-70)	1.16	"	250-800[e]	
5	25.5	5.3	1.42	"	270	257
6	24.4	6.8	1.23	"	240	255
7	23.9	8.5	1.96	"	200	221
8	23.6	6.9	0.61	"	197	225
9	25.7	3.0	1.15	"	196	185
10	24.3	10.7	1.38	"	214	234
11[d]	24.0	7.2	1.26	"	176	193
12	23.7	6.7	1.23	0.284	186	211
13	24.0	7.1	1.20	0.125	222	245
14	24.0	6.8	1.24	0.0404	570	638
15	23.3	6.4	1.24	0.0306	660	810
16	23.0	6.0	1.25	0.0153	1150	1449
17	23.3	3.8	1.22	0.0303	670	822

[a] $(Fe^{++}) = 7.2 \times 10^{-4}$ $\underline{M}$

[b] $(Fe^{++}) = 4.3 \times 10^{-3}$ $\underline{M}$

[c] $(Cl^{-}) = 5.0 \times 10^{-3}$ $\underline{M}$

[d] $\mu = 1.00$

[e] The uncertainty in Q is allowed for in this estimate

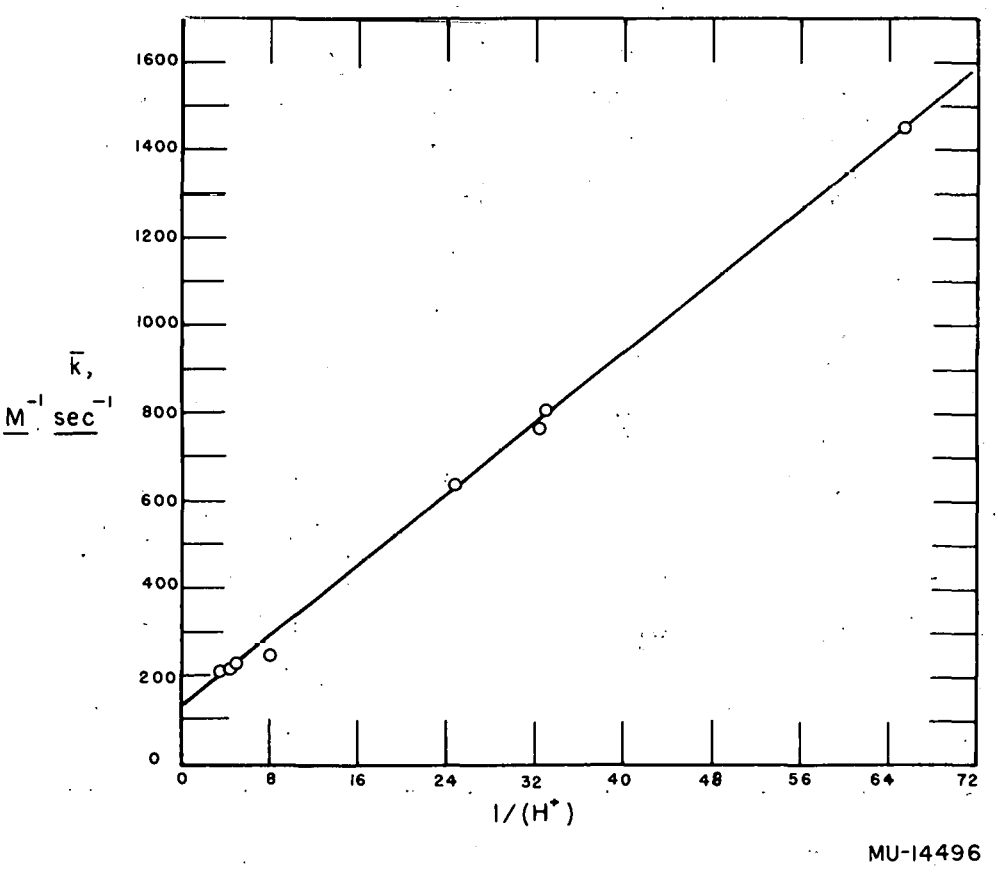

Fig. 9. The acid dependence of $\bar{k}$ at 25°C and μ = 0.40.

Table VI shows a comparison of the various rate quantities obtained in this study with the values obtained earlier by Below.

Table VI

Comparison of rate quantities. ($25^{\circ}C$, $\mu = 0.40$)

	Below	Coppel
$\Delta H_1^{\ddagger}$ (kcal/mole)	10 ± 1	13.0 ± 1.4
$\Delta H_2^{\ddagger}$ (kcal/mole)	24 ± 3	20.2 ± 1.4
$\Delta S_1^{\ddagger}$ (eu)	-15 ± 8	-5 ± 5
$\Delta S_2^{\ddagger}$ (eu)	27 ± 12	15 ± 5
k_1 (M^{-1} sec^{-1})	124 ± 10	127 ± 10
k_2 (sec^{-1})	21 ± 2	20.2 ± 2

Although the two sets of results are consistent if one allows the maximum possible experimental error, the entropy values of Below do not give reasonable comparisons whereas the new values reported here do, as is shown in the discussion to follow.

Discussion

On the assumption that ferric ion and its complexes are hexa-coordinated in aqueous solution, a mechanism consistent with the data can be proposed which consists of the following two paths:

$$\text{(a)}\quad Fe(H_2O)_6^{+++} + SCN^- \underset{k_1'}{\overset{k_1}{\rightleftharpoons}} Fe(H_2O)_5SCN^{++} + H_2O,$$

(b) $Fe(H_2O)_6^{+++} \overset{Q_h}{\rightleftharpoons} Fe(H_2O)_5OH^{++} + H^+$

$Fe(H_2O)_5OH^{++} + SCN^- \overset{k_3}{\rightleftharpoons} Fe(H_2O)_4(OH)SCN^+ + H_2O$

$Fe(H_2O)_4(OH)SCN^+ + H^+ \rightleftharpoons Fe(H_2O)_5SCN^{++}$,

where $k_3 = k_2/Q_h$.

Instead of Mechanism (a), which has an activated complex containing iron of coordination number 7, an alternate mechanism for the first path could be

(c) $Fe(H_2O)_6^{+++} = Fe(H_2O)_5^{+++} + H_2O$

$Fe(H_2O)_5^{+++} + SCN^- \xrightarrow{k} Fe(H_2O)_5SCN^{++}$.

This mechanism requires that the exchange of water molecules in the first coordination sphere with the bulk water molecules be faster than the ferric complexing rate. The only published work on the water exchange shows that the exchange is complete within 3.5 minutes at room temperature in 1.1 M perchloric acid[14] -- a result that does not preclude Mechanism (c). Nuclear magnetic resonance measurements indicate that the water exchange is very much faster than the ferric thiocyanate reaction,[15] and therefore the mechanism is a possible one. In analogy to (c) a mechanism in which water is first eliminated could be written in place of (b).

There appears to be no way at the present time of deciding between these two types of mechanisms for the ferric thiocyanate reaction. In principle the entropies of activation might be used to distinguish between them. The entropy of activation for the seven-coordinated activated complex

would be expected to be appreciably more negative than for the six-coordinated activated complex of the second mechanism, because an additional water molecule is involved in the former. This difference might be as great as 8 eu, as discussed below for paths (a) and (c). The observed entropies of activation seem rather negative, which might be taken as evidence for the seven-coordinated activated complex. The uncertainties in the entropies and the estimation of values expected for the two models is so great, however, that no reliance can be placed on such an argument.

For the base-catalyzed path, mechanisms involving hydroxide could be written, but they seem much less plausible (although not impossible) because of the extremely low concentration of hydroxide ion.

The value of k_3 at 25°C and $\mu = 0.40$ is 1.0×10^4 $\underline{M}^{-1}$ sec^{-1}, compared with $k_1 = 127$ $\underline{M}^{-1}$ sec^{-1}. The greater rate of the catalyzed path may be due to the weakening of the bonding of the hydrated waters by the negative OH^-, thus permitting easier entry of the thiocyanate ion into the coordination sphere. The electrostatic repulsion between the thiocyanate and hydroxide ions would work in the opposite direction. Alternatively, the effect may arise from some interaction of the OH^- with the electronic system of the iron that leads to a more stable activated complex.

In path (a) of the above mechanism, it is observed that the activated complex postulated is somewhat similar in size and charge to the stable end product. Thus a comparison of the entropy of activation with that of the over-all net reaction might be made. Using the value of the complexing constant at $\mu = 0.40$ of 146 and $\Delta H = -1600$ cal/mole previously mentioned, we obtain an entropy for the net reaction of 4.6 eu. The

measured entropy of activation for this path is -5 eu. Since the activated complex has an additional water, coordinated rather than free, and also has one less degree of freedom, these values may well be consistent. For the analogous comparison based on the (c) mechanism it would be difficult to account for -5 eu of activation, but, allowing the maximum uncertainty, the entropy of activation might be as high as zero entropy units, which might be consistent with the (c) mechanism.

Adamson and Wilkins[16] have measured the entropies of activation of the reactions

$$Cr(NH_3)_5SCN^{++} + H_2O \longrightarrow Cr(NH_3)_5H_2O^{+++} + SCN^- ,$$

$$Co(NH_3)_5SCN^{++} + H_2O \longrightarrow Co(NH_3)_5H_2O^{+++} + SCN^- ,$$

for entropies at 25°C of -7.2 and -7.7 eu,* respectively. These should be comparable to the corresponding entropy of activation of the reaction

$$Fe(H_2O)_5SCN^{++} + H_2O \longrightarrow Fe(H_2O)_6^{+++} + SCN^- .$$

The entropy of activation of this reaction can be calculated from ΔS for the equilibrium and the entropy of activation of the reverse reaction, $\Delta S_1^{\ddagger}$. We obtain a $\Delta S^{\ddagger} = -9.6$ eu, which is well within the limits of experimental error in making the comparison.

Bjerrum, Poulsen, and Bjerrum have measured the kinetics[17] of the reaction

$$Cr^{+++} + SCN^- \longrightarrow CrSCN^{++} ,$$

---

*Recalculated assuming a frequency factor of 6.2×10^{12} sec^{-1}.

and from their results we have calculated the entropy of activation to be 0.7 eu. This should be comparable to the -5 eu entropy of activation for path (a) in the ferric thiocyanate mechanism. The agreement lies within the limits of experimental error.

It would be of some interest to compare entropies of activated complexes with the entropies of similar stable complexes. We have considered the following complexing:

$$\text{(d)}\quad Fe^{+++} + F^- = FeF^{++} \quad (\text{for } \Delta S_d = 30 \text{ eu}),$$

$$\text{(e)}\quad FeF^{++} + F^- = FeF_2^{+} \quad (\text{for } \Delta S_e = 23 \text{ eu}),$$

where the S values refer to 25°C and $\mu = 0.50$.[18]

The analogous entropies for the thiocyanate rates are

$$\text{(f)}\quad Fe(H_2O)_6^{+++} + SCN^- \xrightarrow{k_1} Fe(H_2O)_6SCN^{++} \quad (\text{for } \Delta S_1^{\ddagger} = -5 \text{ eu}),$$

$$\text{(g)}\quad Fe(H_2O)_5OH^{++} + SCN^- \xrightarrow{k_3} Fe(H_2O)_5OHSCN^{++} \quad (\text{for } \Delta S_3^{\ddagger} = -7.6 \text{ eu}).$$

The much more positive entropy changes for fluoride complexing are due to the smaller size of the fluoride ion and consequent greater release of water molecules from its field when the oppositely charged ions combine. The difference, however, between thiocyanate and fluoride should be largely eliminated if we subtracted the entropies of Reactions (d) and (e) and compared with the difference of Reactions (f) and (g). The chief difference now is between the effects of fluoride and hydroxide on the entropies. The values $\Delta S_d - \Delta S_e = 7$ eu and $\Delta S_1^{\ddagger} - \Delta S_3^{\ddagger} = 2.6$ eu lie within experimental error.

Part III

KINETICS OF THE FORMATION OF THE FERRIC CHLORIDE COMPLEX

Introduction

No previous work had been reported on the kinetics of the formation of the first ferric chloride complex. This reaction is known to be rapid, and because of its similarity to the corresponding ferric thiocyanate reaction which was investigated earlier in this laboratory, this study was undertaken in order to gain a broader understanding of the kinetics of such complexing reactions.

Equilibrium Quotients

The principal equilibria between ferric and chloride ions in aqueous solution of low chloride concentration are known to be

$$Fe^{+++} + Cl^- = FeCl^{++}, \qquad Q_{1c} = \frac{(FeCl^{++})}{(Fe^{+++})(Cl^-)};$$

$$FeCl^{++} + Cl^- = FeCl_2^+, \qquad Q_{2c} = \frac{(FeCl_2^+)}{(FeCl^{++})(Cl^-)}.$$

Rabinowitch and Stockmayer made an extensive spectrophotometric study of these equilibria and obtained values of Q_{1c} and Q_{2c} at zero ionic strength and 25°C, of 30 ± 5 and 4.5 ± 2 respectively.[19] From their ionic-strength-dependence results they obtained the equation

$$\log Q_{1c} = 1.51 - \frac{3\sqrt{\mu}}{1 + 1.5\sqrt{\mu}} + 0.295\,\mu \qquad (18)$$

for Q_{1c} as a function of ionic strength. Their temperature-dependence results gave a value for ΔH_{1c} of 8.5 ± 0.2 kcal/mole at an ionic strength of 0.61. Olerup obtained a value for Q_{1c} of 5.7 at 20°C and an ionic

strength of 2.0,[20] which is in fair agreement with the results of Rabinowitch and Stockmayer.

Although Rabinowitch and Stockmayer did not take into consideration the polymerization of hydrolyzed ferric ion,[10] it is doubtful that this omission introduced serious errors into their ferric chloride equilibrium-quotient results. These were obtained empirically by comparing the absorption of each chloride solution with the absorption of a similar solution without chloride. Since the total ferric concentration in these experiments was very large compared with the chloride concentration, the fraction of ferric ion complexed was negligible. Therefore, the difference in absorption of the two solutions could be directly attributed to ferric chloride complexes. Also the acidities were such as to make the optical density arising from hydrolyzed species negligible.

The work reported here was carried out at an ionic strength of 1.0. The value of Q_{1c} from Eq. (18) is 4.03. This high ionic strength (as compared with 0.40 used in the ferric thiocyanate study) was necessary because of the high acidities required to eliminate absorption due to hydrolyzed ferric species, which absorb appreciably in the region of ferric chloride absorption.

The ΔH reported by Rabinowitch and Stockmayer was not used in this work because in the experiments from which their value was calculated a large excess of chloride ion was used, as a result of which more than 20% of the total ferric ion would be present as $FeCl^{++}$ and 1% as $Fe(Cl)_2^{+}$. Under these conditions the calculations indicated in their paper would not yield accurate equilibrium quotients. Since no other value was available, it was necessary to remeasure this quantity.

A ferric chloride solution was prepared containing 0.01222 $\underline{M}$ $Fe(ClO_4)_3$,

0.0111 M NaCl, and 1.298 M $HClO_4$, giving an ionic strength of 1.382. Equilibrium quotients for hydrolysis and dimerization were calculated from the ionic-strength-dependence equations of Milburn and Vosburgh.[10] By use of these values of $Q_h = 1.53 \times 10^{-3}$ and $Q_d = 886$, and the molar extinction coefficients for Fe^{+++}, $FeOH^{++}$, $Fe_2(OH)_2^{+4}$, and $FeCl^{++}$ (discussed later), Q_{1c} can be determined as a function of temperature by optical density measurements.

The wave length used was 370 mμ where the total optical density due to Fe^{+++}, $FeOH^{++}$, and $Fe_2(OH)_2^{+4}$ was less than 4% of the total optical density. Furthermore, the amount of ferric ion hydrolyzed and complexed is very small (about 6%), and corrections on (Fe^{+++}) become almost negligible. It was assumed that the molar extinction coefficients did not change with temperature or with ionic strength.

The measurements were made on a Beckman Model DU spectrophotometer with a thermostated cell holder. The temperature in the cell was held constant to $\pm$ 0.1° over a temperature range from 22° to 45°C. The temperatures were measured to $\pm$ 0.02° with a thermistor placed inside the cell so as to be in contact with the solution but not interfering in the light path. Figure 10 shows a plot of log Q_{1c} versus $1000/T^{\circ}K$. The data fall on a straight line, the slope of which gives ΔH_{1c} = 6.0 $\pm$ 0.1 kcal/mole. This value is significantly different from the value of 8.5 $\pm$ 0.2 reported by Rabinowitch and Stockmayer.

Values of Q_{2c} and ΔH_{2c} were not required, since conditions were chosen so as to make formation of $Fe(Cl)_2^+$ negligible in all runs.

It was again necessary to correct all rate data for the hydrolysis of ferric ion, although (as is shown later) this correction is much less significant for the ferric chloride results than it was for the

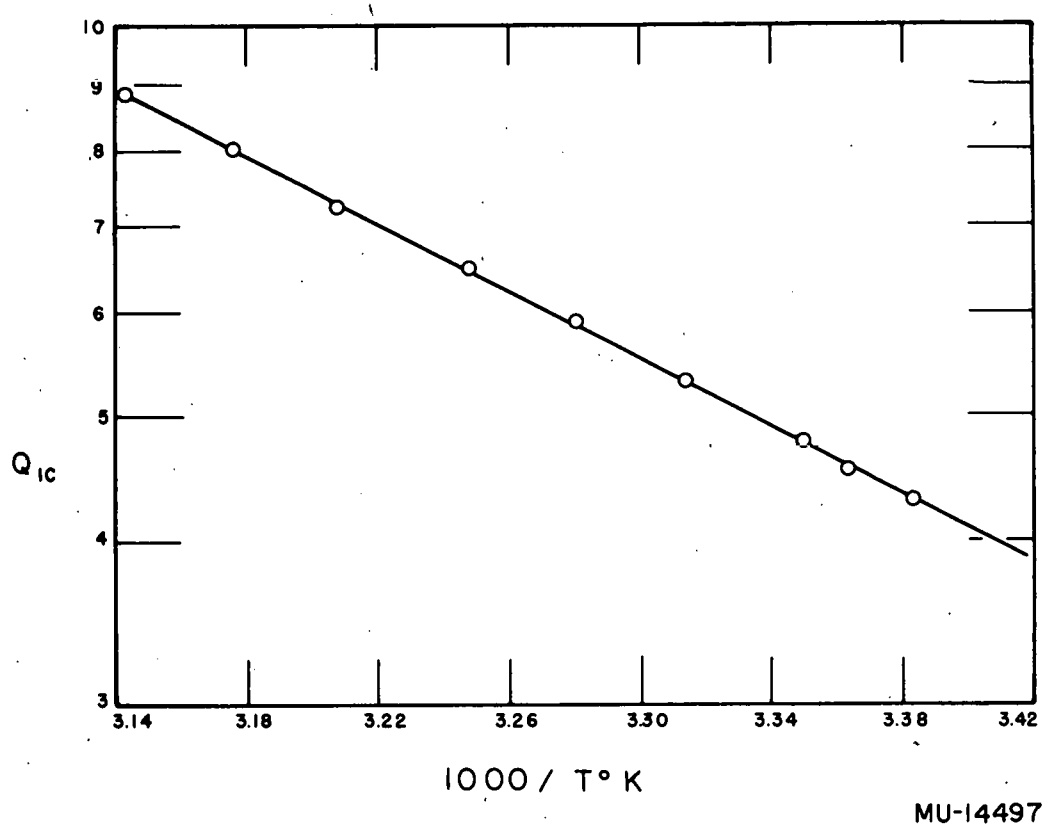

Fig. 10. The temperature dependence of Q_{1c}.

ferric thiocyanate work. The equilibrium quotients Q_h and Q_d as defined earlier in Part II were again obtained from the work of Milburn and Vosburgh.[10] From these data we have Q_h ($25^\circ C$, $\mu = 1.0$) = 1.65×10^{-3} and Q_d ($25^\circ C$, $\mu = 1.0$) = 711. The values of ΔH_h = 10.2 kcal/mole and ΔH_d = -8.2 kcal/mole were again used to correct Q_h and Q_d for temperature changes.

Molar Extinction Coefficients

In the calculations of the kinetic runs it was necessary to know the molar-extinction coefficients of all species present in the reacting solutions. Rabinowitch and Stockmayer's spectrophotometric study was primarily at wave lengths above 400 mμ. Also, they did not allow for the presence of $Fe_2(OH)_2^{+4}$. In this wave length region the absorption due to $FeCl^{++}$ is not large enough under the experimental conditions used here to allow accurate observation of $FeCl^{++}$ formation with the rapid-recording spectrophotometer. It was therefore necessary to measure the molar extinction coefficients in the spectral region to be used, i.e., 300 to 400 mμ.

Three solutions were prepared, each containing 0.003764 M $Fe(ClO_4)_3$ and each at an ionic strength of 1.15. These solutions had hydrogen ion concentrations (uncorrected for hydrolysis) of 0.250, 0.0528, and 0.0308. From Milburn's and Vosburgh's values for Q_h and Q_d, the concentrations of Fe^{+++}, $FeOH^{++}$, and $Fe_2(OH)_2^{+4}$ were calculated. The optical densities of these solutions were then measured on a Beckman Model DU spectrophotometer at $25.0^\circ C$. The cells were fused quartz with a 2.000-cm light path and were thermostated in a water-jacketed cell holder. The temperature inside the cells was $25.0 \pm 0.1^\circ C$. Milburn and Vosburgh had reported molar extinction coefficients for the three ferric species at 340 mμ. These

were $(Fe^{+++}) = 2.84$, $(FeOH^{++}) = 925$, and $(Fe_2(OH)_2^{+4}) = 3000$. A check on the experimental results was made by calculating the optical density of the three solutions and comparing the results with those obtained experimentally. The results are shown below.

(H^+)	D_{exp}	D_{calc}
0.250	0.068	0.0682
0.0528	0.276	0.280
0.0308	0.512	0.512

By use of the calculated concentrations of Fe^{+++}, $FeOH^{++}$, and $Fe_2(OH)_2^{+4}$ and the measured optical-density values for the three solutions, the molar-extinction coefficients shown in columns 2, 3, and 4 of Table VII were obtained.

To obtain the molar extinction coefficients for $FeCl^{++}$ a solution identical to the high-acid solution (0.250 M H^+) used above was made, with the addition of 0.0555 M NaCl. It can be shown that under these conditions higher chloride complexes (i.e., $FeCl_2^+$) may be neglected. Using Rabinowitch's and Stockmayer's value for Q_{2c} one sees that the concentration of $FeCl_2^+$ is only about 5% of the concentration of $FeCl^{++}$, and since the molar extinction coefficients are of the same order of magnitude, $FeCl_2^+$ may be neglected. The measured optical-density values and the calculated values of Q_h, Q_d, Q_{1c}, ϵ_f, ϵ_h, ϵ_d, (see key in Table VII) gave the molar extinction coefficient values for $FeCl^{++}$ shown in column 5 of Table VII.

Although this method of obtaining the molar extinction coefficients is not highly precise, it does give a consistent set of values which may

Table VII

Molar extinction coefficients

Key to extinction coefficient subscripts:

$f = Fe^{+++}$, $h = FeOH^{++}$, $d = Fe_2(OH)_2^{+4}$, $c = FeCl^{++}$

λ (mμ)	ϵ_f	ϵ_h	ϵ_d	ϵ_c	ϵ_f^a	ϵ_h^a	ϵ_d^a	ϵ_f^b	ϵ_c^b	ϵ_c^*
400	0.499	53.8	29.6	127				0.225	128	100
390	0.607	81.4	148	238						200
380	0.631	129	428	428						450
370	0.996	194	1030	702						750
360	1.59	346	1750	1060	0.90					1000
350	1.97	545	2720	1440	1.20					1300
340	3.69	811	3520	1680	2.84	925	3000			1450
330	8.35	1100	3620	1690	7.30					1300
320	20.6	1440	2920	1470	20.2					1250
310	55.5	1700	2240	1120						1000
300	129	1790	2790	945				134		

a - Milburn and Vosburgh[10]

b - Rabinowitch and Stockmayer[19]

* - Olerup[20]

be used to check optical densities of experimental solutions. The values reported in Table VII are probably given to more significant figures than the experimental accuracy would justify. They were used to this accuracy because they have been considered as an internally consistent set for this experimental work. Comparable values by other workers are shown in columns 6 - 11, Table VII, and these indicate satisfactory agreement within experimental limits of error. The values obtained by Olerup are reported here very roughly, because they had to be read from a small scale plot.

These molar extinction coefficients were checked several times in later experiments by making known solutions and comparing experimental and calculated optical densities, and the agreement was usually within 2%.

Reagents

All reagents used in this work were similar to those used in the ferric thiocyanate experiments (see Part II), with the exception of the sodium chloride solution.

A stock solution of approximately 0.3 M sodium chloride was prepared by drying the analytical reagent salt at 110°C, then dissolving a weighed amount of the salt in the desired amount of distilled water. Aliquot portions of the resulting solution were dried and weighed and the concentration was compared with that calculated from the initial gross weighing. A further check was made by precipitating the chloride with silver nitrate solution and weighing the silver chloride precipitate. All three values agreed within 0.2%.

Rate Law

As a reasonable working hypothesis, it was assumed that the rate law for the ferric chloride complex formation was analogous to that for the

ferric thiocyanate reaction, where at constant hydrogen ion concentration the mechanism can be written as

$$Fe^{+++} + Cl^{-} \underset{\bar{k}'}{\overset{\bar{k}}{\rightleftharpoons}} FeCl^{++} \; ; \qquad (19)$$

the integrated rate law is

$$-\bar{k}t = \frac{2.30}{(Fe^{+++}) + 1/Q_{1c}} \log \frac{(FeCl^{+++})_{\infty} - (FeCl^{++})}{(FeCl^{++})_{\infty} - (FeCl^{++})_{o}} \; , \qquad (20)$$

where (Fe^{+++}) has been assumed to be constant. Under the experimental conditions of this study, with a value of Q_{1c} of approximately 4 and ferric and chloride ion concentrations of 8×10^{-3} M and 4×10^{-3} M respectively, very little of either the ferric ion or chloride ion is complexed. This means that the linearity of a plot of log $[(FeCl^{++})_{\infty} - (FeCl^{++})]$ versus time is not a good measure of the assumed order of reaction. It can, however, be shown that the linearity of such a plot does indicate a first-order dependence on $(FeCl^{++})$ for the reverse rate; from the known form of the equilibrium quotient one sees that there must be a first-order dependence on ferric and chloride ions for the forward rate. The rate law for Eq. (19) can be written as

$$\frac{d(FeCl^{++})}{dt} = \bar{k}\,(Fe^{+++})(Cl^{-}) - \bar{k}'\,(FeCl^{++}).$$

Assuming both (Fe^{+++}) and (Cl^{-}) to be constant and integrating, one obtains

$$-\bar{k}'t = \log \frac{(FeCl^{++})_{\infty} - (FeCl^{++})}{(FeCl^{++})_{\infty} - (FeCl^{++})_{o}} \; .$$

This indicates that a plot of log $[(FeCl^{++})_{\infty} - (FeCl^{++})]$ versus time should give a straight line where $\bar{k}' = -2.03 \times$ slope. Such plots of the experimental data were in general linear; there were some random deviations

due to various experimental limitations.

Further verification of order with respect to ferric and chloride ion concentrations was obtained by varying the concentrations of these ions and comparing the $\bar{k}$ values calculated by use of Eq. (20).

Calculation of $\bar{k}$

Values of $\bar{k}$ were obtained from Eq. (20). Since we have $\bar{k} = \frac{-2.30 \times \text{slope}}{(Fe^{+++}) + 1/Q_{1c}}$, as was the case for the ferric thiocyanate reaction, again the only experimental quantity required other than the slope is (Fe^{+++}). However, this quantity is now almost negligible, i.e., about 4% of Q_{1c}, and it is not necessary to know it with any great accuracy nor to know the mixing ratio accurately.

Although no further experimental data were necessary in order to calculate $\bar{k}$, it was desirable to provide some type of measurement to check the experimental conditions. After each run a 10-ml sample was removed from the mixing apparatus, and brought to 25°C. The mixer was then filled with water and placed in the spectrophotometer, and a blank value was put onto the negative. The blank was also removed from the mixer. The optical densities of the sample and the blank were then measured on a Cary spectrophotometer at the appropriate wave length. The measured optical density of the sample versus blank was then compared with the value calculated from the negative by the equation

$$D = \log x_b/x \ .$$

The agreement was in general good to about 5%, and this was taken as evidence that the sample removed is a good measure of the final equilibrium state of the sample observed kinetically during the run.

A portion of the removed sample was then analyzed for total Fe(III) by the spectrophotometric thiocyanate method described earlier (Part II). From the known total Fe(III) and the known initial concentration in the ferric solution a mixing ratio was calculated, and in turn the total chloride ion concentration was obtained. From the total Fe(III) and Cl^- concentrations and the equilibrium quotients for hydrolysis, dimerization, and complexing, the concentrations of Fe^{+++}, $FeOH^{++}$, $Fe_2(OH)_2^{+4}$, and $FeCl^{++}$ were calculated. From these and the previously measured molar extinction coefficients (Table VII) the total optical density of the sample was obtained and compared with that measured on the Cary spectrophotometer. This comparison was generally good to about 5%, indicating that the sample composition was that expected.

Ferric and Chloride Dependence

Table VIII shows the data for runs made at varying ferric and chloride ion concentrations. Runs IV-54, IV-58, IV-67, and VI-72 show that a twofold change in ferric concentration has a very small effect on the rate constant, and considering an estimated uncertainty in $\bar{k}$ of about 10%, the differences are negligible. Run V-34, which is at a fourfold increase in chloride ion concentration and at a fourfold decrease in ferric ion concentration, also lies within experimental error of the other runs. These runs were at a high hydrogen ion concentration (0.90 M).

Because the mechanism involves a base-catalyzed path, as indicated by the larger $\bar{k}$ value in run VI-61 at hydrogen ion concentration of 0.156 M, it was also necessary to check the ferric and chloride dependence at lower acidities. Runs VI-61, VI-85, VII-8, and VII-6 indicate no change in rate constant over a fourfold dilution in ferric ion concentration, in runs at

Table VIII

Kinetic data on ferric and chloride dependence (for $\mu = 1.0$)

Expt	Temp ($^{\circ}$C)	ΣFe(III) ($\underline{M} \times 10^{3}$)	ΣCl^{-1} ($\underline{M} \times 10^{3}$)	(H^{+}) ($\underline{M}$)	$\bar{k}$ ($\underline{M}^{-1}$ sec^{-1})	$\bar{k}$ (25°) ($\underline{M}^{-1}$ sec^{-1})
IV-54	24.11	9.8	4.3	0.89	26.8	29.9
IV-58	23.7	9.5	4.3	0.89	25.0	29.4
IV-67	23.41	5.0	4.0	0.90	22.6	27.4
V-34	22.06	2.0	18.5	0.90	20.0	28.7
VI-72	22.96	5.6	5.3	0.90	20.1	26.2
VI-61	22.41	8.5	4.7	0.156	88.5	125.8
VI-85	23.68	8.2	4.6	0.156	95.0	113.2
VII-8	25.75	1.7	4.5	0.156	130.1	118.0
VII-6	24.80	1.7	4.5	0.156	109.1	112.0
VII-37	22.8	3.1	15.9	0.0622	183	261
VII-49	27.9	8.1	4.7	0.0622	259	227
VII-54	26.6	3.4	15.4	0.0622	228	253

0.156 $\underline{M}$ hydrogen ion concentration. Runs VII-37, VII-49, and VII-54 show no effect on $\bar{k}$ at $(H^{+}) = 0.0622$ $\underline{M}$, with fourfold dilution of chloride ion and threefold increase in ferric ion.

These results in conjunction with the linearity of the log $[(FeCl^{++})_{\infty} - (FeCl^{++})]$ plots are taken as evidence for the first-order dependence on ferric and chloride ion concentration.

The $\bar{k}$ values at 25°C in column 7 of Table VIII were calculated from those in column 6 by use of the $\Delta H^{\ddagger}$ values, which are discussed in the section on temperature dependence.

Acid Dependence

Table IX shows the results of runs made at varying hydrogen ion concentrations and Fig. 11 shows a plot of $\bar{k}$ (25°C) versus $1/(H^+)$. At high values of (H^+) (that is, 0.90 to 0.20 M) the plot is analogous to the hydrogen ion dependence results of the ferric thiocyanate reaction -- i.e., a linear relationship with a finite intercept at $1/(H^+) = 0$ -- and can be interpreted as representing the rate law

$$\frac{d(FeCl^{++})}{dt} = k_1(Fe^{+++})(Cl^-) + k_2 \frac{(Fe^{+++})(Cl^-)}{(H^+)} ,$$

where $\bar{k} = k_1 + k_2/(H^+)$.

The values used for $\bar{k}$ at $(H^+) = 0.900$ and 0.311 were taken from Fig. 13 of the temperature-dependence study, which is discussed in the following section. These values were given more weight than those obtained from single runs because they represent entire series of runs.

It is seen that at the lower hydrogen ion concentrations (0.156 M and particularly 0.0622 M) deviations from the linear relationship appear. At these lower acidities several series of runs gave low rate constants when fresh solutions were used, and the rate constant appeared to increase as the solutions were aged. Although the low rate constants for fresh solutions were first believed to be outside of experimental error, since they were as much as 25% below results for aged solutions, when experiments were repeated on fresh solution no abnormally low rate constants were observed. It was therefore concluded that the aging effect was not real and must be ascribed to experimental error.

It was observed that the rate constants at low hydrogen ion concentration, regardless of aging or experimental error, were still lower than the expected $1/(H^+)$ extrapolation. This is due to mixing limitations

Table IX

Acid-dependence results (for μ = 1.0)

Expt	Temp (^{o}C)	(ΣFe(III))[a] ($\underline{M}$ x 10^{3})	(ΣCl^{-})[a] ($\underline{M}$ x 10^{3})	(H^{+}) ($\underline{M}$)	$\bar{k}$ ($\underline{M}^{-1}$ sec^{-1})	$\bar{k}$ (25^{o}) ($\underline{M}^{-1}$ sec^{-1})
	25.0			0.90		28.8
	25.0			0.311		66.1
IV-91	25.03	9.6	4.0	0.702	38.0	38.0
V-3	23.94	7.9	4.8	0.428	49.0	57.1
V-8	23.6	8.7	4.4	0.328	54.8	65.8
V-11	23.56	9.6	4.1	0.209	78.6	94.9
V-14	22.97	8.3	4.6	0.209	72.0	92.2
VI-21	25.67	7.7	4.8	0.328	74.9	68.8
VI-25	28.19	8.5	5.2	0.209	151.6	100.0
VI-34	27.18	8.8	5.0	0.733	44.7	34.2
VI-37	24.10	8.6	4.7	0.447	44.4	49.9
VI-40	24.51	9.0	4.5	0.428	49.1	52.3
VI-61	22.41	8.5	4.7	0.156	88.5	125.8
VI-85	23.68	8.2	4.6	0.156	95.0	113.2
VII-8	25.75	1.7	4.5	0.156	130.1	118.0
VII-6	24.80	1.7	4.5	0.156	109.1	112.0
VII-37	22.35	3.1	15.9	0.0622	183	261
VII-49	26.00	8.1	4.7	0.0622	259	227
VII-54	24.26	3.4	15.4	0.0622	228	253

[a]Total stoichiometric concentration

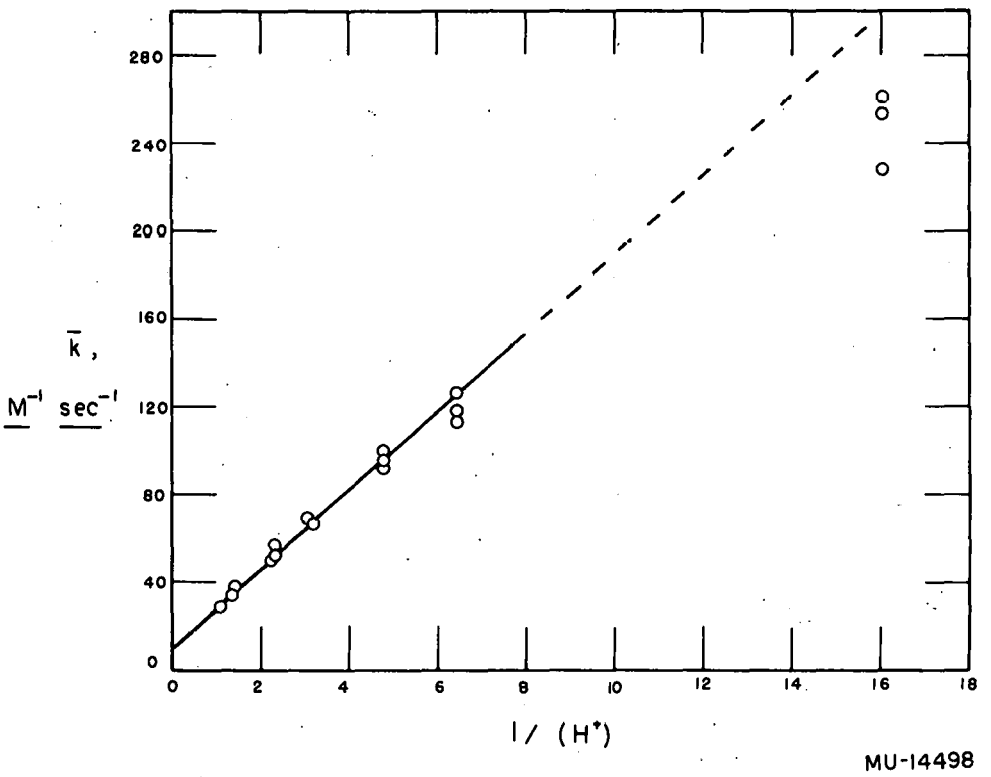

Fig. 11. The acid dependence of $\bar{k}$ at 25°C and μ = 1.0.

which become important under these conditions. At 0.0622 M (H^+) the slope of the log plot used in calculating $\bar{k}$ was severely limited by mixing times. At sweep frequencies of 60 cycles per second a reaction could be observed for only about two sweeps at this low hydrogen ion concentration. In mixing experiments (see Part I) the mixing process itself took 16 milliseconds (one sweep) for 83% mixing. Fig. 12 shows the plot of log $[(FeCl^{++})_\infty - (FeCl^{++})]$ versus time for a run at 0.0622 $\underline{M}$ (H^+). It is evident that the early data are being severely limited by mixing.

The values of $\bar{k}$ at 25°C in Table IX and Fig. 11 were calculated by use of the $\Delta H^{\ddagger}$ values to be discussed in the following section. The slope and zero intercept of Fig. 11 give values of $k_2 = 18.0$ sec^{-1} and $k_1 = 9.4$ $\underline{M}^{-1}$ sec^{-1}.

Temperature Dependence

To determine the heats and entropies of activation a series of experiments was run covering the temperature range 16°C to 32°C, and the results are shown in Table X. Because of the hydrogen ion dependence of $\bar{k}$ the runs were made at two acidities. Figure 13 shows a plot of log $\bar{k}$ /T°K versus 1000/T°K for the two acidities. Since the data showed no signs of specific curvature, the best-fitting straight lines were drawn. The average deviation from these lines is less than 5%. Values of $\bar{k}$ were taken from this plot at three temperatures corresponding to 1000/T°K = 3.28, 3.36, and 3.44, and from these were calculated values of k_1 and k_2 at these three temperatures. Figure 14 shows a plot of log $k_1/T^\circ K$ versus 1000/T°K and similarly for k_2. From the slopes of these lines, the values $\Delta H_1^{\ddagger} = 16.6 \pm 2.0$ kcal/mole and $\Delta H_2^{\ddagger} = 23.3 \pm 2.0$ kcal/mole

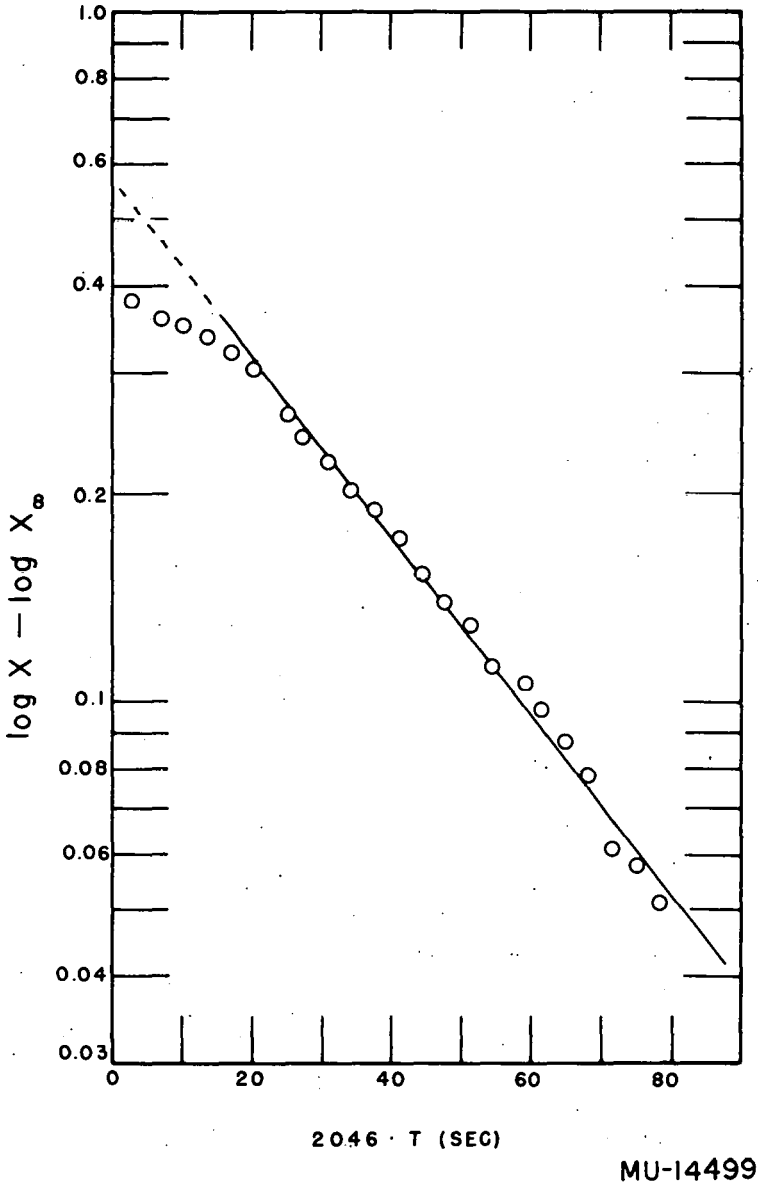

Fig. 12. The kinetic curve of experiment VII-54, Table IX.

Table X

Temperature-dependence data (at μ = 1.0)

Expt	Temp (^{o}C)	ΣFe(III)[a] ($\underline{M} \times 10^{3}$)	(ΣCl^{-})[a] ($\underline{M} \times 10^{3}$)	(H+) ($\underline{M}$)	$\bar{k}$ ($\underline{M}^{-1}$ sec^{-1})
IV-54	24.11	9.8	4.3	0.89	26.8
IV-58	23.7	9.5	4.3	0.89	25.0
IV-67	23.41	5.0	4.0	0.90	22.6
IV-84	31.29	6.3	4.9	0.90	59.3
IV-87	31.74	6.6	4.7	0.90	66.5
V-34	22.06	2.0	18.5	0.90	20.0
VI-68	23.95	6.9	4.6	0.90	24.8
VI-72	22.96	5.6	5.3	0.90	20.1
VII-90	18.16	6.4	4.8	0.90	12.2
VII-93	15.97	8.0	4.7	0.90	9.45
VII-95	31.72	7.8	4.8	0.90	69.1
IX-31	25.03	8.0	4.8	0.90	30.4
IX-33	22.23	8.0	4.7	0.90	20.0
IX-15	31.45	7.9	4.7	0.311	154.7
IX-17	16.97	7.6	4.8	0.311	23.0
IX-19	24.00	7.8	4.7	0.311	62.9
IX-23	18.40	7.6	4.8	0.311	28.2
IX-25	21.23	7.7	4.8	0.311	40.5
IX-27	26.24	7.5	4.9	0.311	74.3
IX-29	32.28	7.4	4.9	0.311	161.2

[a]Total stoichiometric concentration

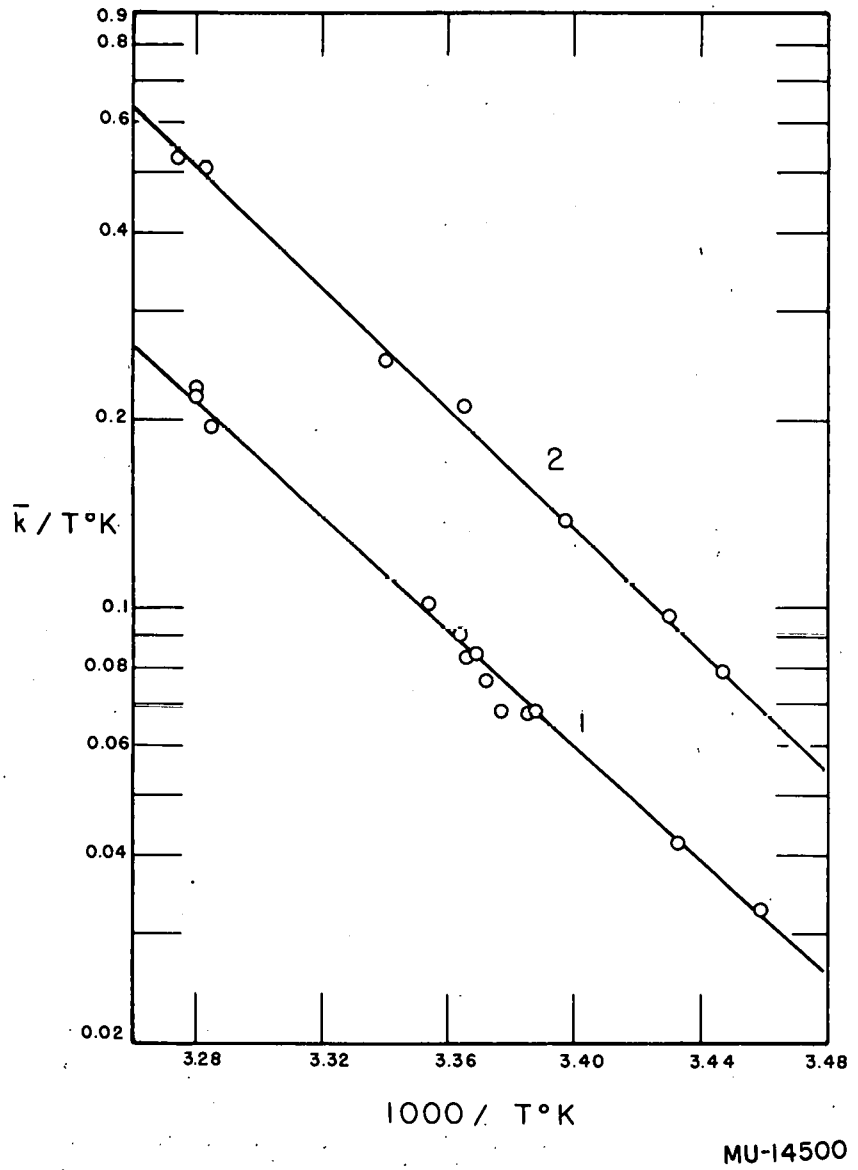

Fig. 13. The temperature dependence of $\bar{k}$, Curve 1 (H^+) = 0.90, Curve 2 (H^+) = 0.311.

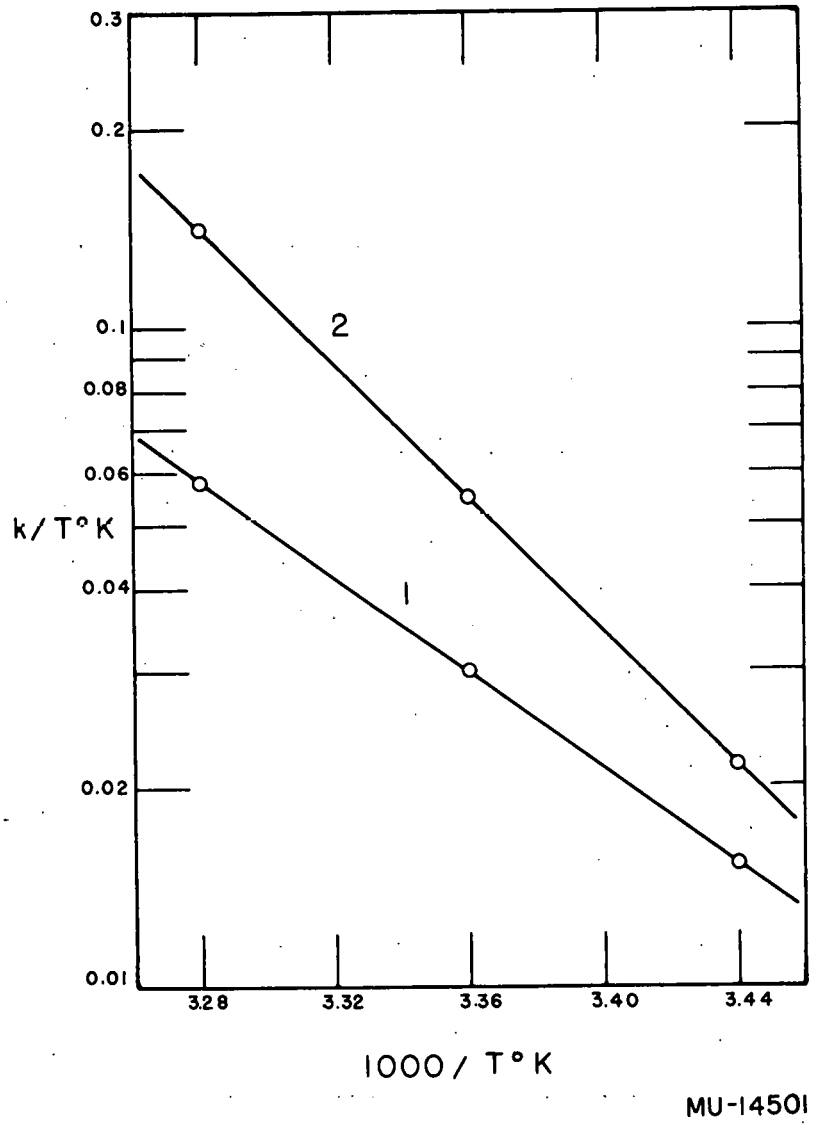

Fig. 14. The temperature dependence of k_1 (Curve 1), and k_2 (Curve 2).

were calculated. The corresponding entropies of activation at 25°C were calculated and found to be $\Delta S_1^{\ddagger} = 2 \pm 6$ eu and $\Delta S_2^{\ddagger} = 25 \pm 6$ eu. The values of $k_1 = 9.4\ \underline{M}^{-1}\ sec^{-1}$ and $k_2 = 17.5\ sec^{-1}$ from this plot are in good agreement with the values of 9.4 and 18.0 obtained from the hydrogen ion dependence results.

The uncertainties were obtained by assuming a possible error of 10% in the rate constants at the high and low temperatures.

Discussion of the Rate Law

Table XI shows a comparison of the final kinetic results for the complexing of ferric ion by thiocyanate and chloride ions.

Table XI

Comparison of thiocyanate and chloride results at 25°C

		Thiocyanate[a]	Chloride[b]
$\Delta H_1^{\ddagger}$	kcal/mole	13.0 ± 1.4	16.6 ± 2.0
$\Delta H_2^{\ddagger}$	kcal/mole	20.2 ± 1.4	23.3 ± 2.0
$\Delta S_1^{\ddagger}$	eu	-5 ± 5	2 ± 6
$\Delta S_2^{\ddagger}$	eu	15 ± 5	25 ± 6
$k_1\ \underline{M}^{-1}$	sec^{-1}	127 ± 10	9.4 ± 1
k_2	sec^{-1}	20.2 ± 2	18.0 ± 2

[a] $\mu = 0.40$

[b] $\mu = 1.0$

On the basis of the data, a mechanism analogous to the thiocyanate reaction can be proposed:

$$(a')\quad Fe(H_2O)_6^{+++} + Cl^- \underset{k_1'}{\overset{k_1}{\rightleftharpoons}} Fe(H_2O)_5Cl^{++} + H_2O$$

$$(b')\quad Fe(H_2O)_6^{+++} \overset{Q_h}{\rightleftharpoons} Fe(H_2O)_5OH^{++} + H^+,$$

$$Fe(H_2O)_5OH^{++} + Cl^- \underset{k_3'}{\overset{k_3}{\rightleftharpoons}} Fe(H_2O)_4OHCl^+ + H_2O$$

$$Fe(H_2O)_4OHCl^+ + H^+ \rightleftharpoons Fe(H_2O)_5Cl^{++},$$

where $k_3 = k_2/Q_h$.

Also a mechanism involving the hexacoordinated activated complex (Mechanism (c) in Part II), where water is released before the complexing ligand enters, could be proposed. However, as mentioned earlier, the entropy of activation for the seven-coordinated activated complex would be expected to be appreciably more negative than for the six-coordinated one, which in turn should be comparable to the over-all equilibrium entropy. The values $\Delta S_{1c}^{\ddagger} = 2$ eu (25°, $\mu = 1.0$) and $\Delta S_{1c} = 23$ eu (25°, $\mu = 1.0$) give some, although not conclusive, support to the seven-coordinated activated complexes (Mechanisms (a') and (b')). The ΔS_{1c} value given above is based on the ΔH_{1c} value determined by a single experiment in this work.

In comparing the entropy of activation results of the thiocyanate and chloride reactions (see Table XI), it is seen that the chloride entropies are more positive by about 7 to 10 entropy units than the analogous thiocyanate values. The larger ionic strength at which the chloride values were determined cannot be the cause of this difference. At lower ionic strengths the chloride entropies would be expected to be even more positive. This difference is probably due to the stronger hydration of chloride ion

and a correspondingly greater release of water molecules when the activated complex is formed. A similar trend is observed in the equilibrium entropies.

The value of k_3 (chloride) at 25°C and μ = 1.0 is 1.1 x 10^4 $\underline{M}^{-1}$ sec^{-1}, compared to k_1 (chloride) = 9.4 $\underline{M}^{-1}$ sec^{-1}. On a purely electrostatic argument one would expect the path through $FeOH^{++}$ to be slower than that through Fe^{+++}, which is opposite to the observed result. In the thiocyanate results also one had this same contradiction, which was interpreted as possibly being due to the weakening of the bonding of the hydrated waters by the negative OH^-, thus permitting easier entry of the thiocyanate ion into the coordination sphere. In comparing the rate constants for the uncatalyzed path, k_1 (thiocyanate) = 127 $\underline{M}^{-1}$ sec^{-1} and k_1 (chloride) = 9.4 $\underline{M}^{-1}$ sec^{-1}, one observes a similar trend, although not as pronounced. The more stable and therefore more strongly bonded thiocyanate complex forms more rapidly than the chloride complex, which again is opposite to what one might predict on a purely electrostatic model, where the charge distribution on the polyatomic thiocyanate group would tend to give a smaller attraction and therefore a smaller rate. A comparison of rate constants for the catalyzed path, k_3 (thiocyanate) = 1.0 x 10^4 $\underline{M}^{-1}$ sec^{-1}, k_3 (chloride) = 1.1 x 10^4 $\underline{M}^{-1}$ sec^{-1}, shows no trend and may imply that the effect of OH^- weakening of water bonding predominates over individual ligand bond differences. The agreement in this case could be purely fortuitous and one need not expect the rate constants for similar base-catalyzed ferric-complexing reactions to be equal to those for thiocyanate and chloride ions.

A final comparison can be made between the values of $\Delta S_1^{\ddagger} - \Delta S_3^{\ddagger} =$ -1 eu (chloride), $\Delta S_1^{\ddagger} - \Delta S_3^{\ddagger} = 2.6$ eu (thiocyanate), and $\Delta S_d - \Delta S_e =$ 7 eu (these refer to the ferric fluoride complexes discussed in Part II), and it is seen that all three values lie within the experimental error of one another, and that the agreement between the two kinetic results is better than with the equilibrium value, as might be expected.

No comparisons of the chloride results have been made with analogous kinetic studies by other workers, as was done for the thiocyanate discussion, because such comparable rate studies have not been reported.

Rate of Chloride Complexing from NMR Measurements

It is known that the presence of paramagnetic ions in solution causes a broadening of nuclear magnetic resonance absorption lines. This is due to the deexcitation of the nuclear spin states by the changing local fields of the paramagnetic ion. It is possible to measure lifetimes of excited states from such line broadening.

Wertz[21] has measured the broadening of the Cl^{35} resonance by several paramagnetic ions. Ferric ion showed a very large broadening effect, whereas chromic ion showed no broadening effect. Since chromic chloride complexes are known to form and exchange very slowly, it may be assumed that the chloride needs to enter the first coordination sphere to become deexcited. One can then assume that the rate of deexcitation of chloride is comparable to the rate at which ferric chloride complexes are forming.

Wertz found that the broadening due to 0.1 M ferric ion in 3.0 M sodium chloride was 2.7 gauss, or, in terms of frequency, 1.13×10^3 sec^{-1}. Repeating his experiments, we obtained a broadening of 1.4×10^3 sec^{-1}. This value may still include some instrumental broadening.

Using the relationship of Bruce, Norberg, and Weissman,[22]

$$k = \frac{\pi\Delta\nu}{\sqrt{3}}, \tag{21}$$

where $\Delta\nu$ is the full width at half maximum intensity of the resonance broadening and k is a first-order rate constant for the deexcitation of chlorine nuclei, one obtains $k = 2.0 \times 10^3$ sec^{-1} and 2.5×10^3 sec^{-1} for the two values of $\Delta\nu$ stated above.

Gamlen and Jordan[23] showed that in 3 $\underline{M}$ Cl^-, and 0.1 $\underline{M}$ Fe^{+++}, the complexes present were 10% $FeCl^{++}$, 20% $Fe(Cl)_2^+$, and 70% $Fe(Cl)_3$. Under these conditions the principal mechanism for exchange and deexcitation of chloride is likely to be

$$Fe(Cl)_2^+ + Cl^{-*} \xrightarrow{k'} Fe(Cl)_3 ,$$

where Cl^{-*} represents excited chlorine nuclei. Then we have

$$-\frac{d(Cl^{-*})}{dt} = k'(Cl^{-*})(Fe(Cl)_2^+) = k\,(Cl^{-*})$$

and

$$k' = k/(Fe(Cl)_2^+).$$

Using the values of k and $(Fe(Cl)_2^+)$ given above, one obtains values of k' of 1×10^5 $\underline{M}^{-1}$ sec^{-1} and 1.3×10^5 $\underline{M}^{-1}$ sec^{-1}.

In this study the following rate constants were measured:

$$Fe^{+++} + Cl^- \xrightarrow{k_1} FeCl^{++}, \qquad k_1 = 9.4\ \underline{M}^{-1}\ \text{sec}^{-1};$$

$$FeOH^{++} + Cl^- \xrightarrow{k_3} FeOHCl^+, \qquad k_3 = 1.1 \times 10^4\ \underline{M}^{-1}\ \text{sec}^{-1}.$$

These comparisons indicate that the rate constant for addition of a third chloride to ferric ion would be roughly 10^4 times that for the first chloride and roughly 10 times that for adding a chloride to a ferric ion with an OH^- already added. On the basis of the hydroxide catalysis of the first ferric chloride complex formation it is not too unreasonable to expect that the presence of chloride on the ferric ion would also catalyze further substitution. The values of k from the NMR measurements and k_3 from the kinetic studies do not offer any immediate inconsistencies.

ACKNOWLEDGMENTS

I would like to express my sincere appreciation to Professor Robert E. Connick for his advice, guidance, and inspiration in connection with so many parts of this research; to Mrs. Jane Waite and Mr. Paul Pfaendtner for contributions to the progress of this project; and to my fellow graduate students who have been a constant source of encouragement.

Financial support was received through the University of California Radiation Laboratory from the U. S. Atomic Energy Commission.

BIBLIOGRAPHY

1. John F. Below, Rapid Reactions: Kinetics of the Formation of the Ferric Thiocyanate Complex (Thesis), UCRL-3011, June 1955.

2. L. R. Ingersoll, O. J. Zobel, and A. C. Ingersoll, Heat Conduction (University of Wisconsin Press, Madison, 1954).

3. R. E. Emmert and R. L. Pigford, Chem. Eng. Progr. 50, 87 (1954).

4. R. T. Knapp, Proc. Inst. Mech. Engrs. (London) A166, 150 (1952).

5. M. S. Plesset, Jour. of Appl. Mech. 16, 277 (1949).

6. R. H. Betts and F. S. Dainton, J. Am. Chem. Soc. 75, 5721 (1953).

7. H. S. Frank and R. L. Oswalt, J. Am. Chem. Soc. 69, 1321 (1947).

8. G. S. Laurence, Trans. Faraday Soc. 52, 236 (1956).

9. M. W. Lister and D. E. Rivington, Can. J. Chem. 33, 1572 (1955).

10. R. M. Milburn and W. C. Vosburgh, J. Am. Chem. Soc. 77, 1352 (1955).

11. T. H. Siddall and W. C. Vosburgh, J. Am. Chem. Soc. 73, 4270 (1951).

12. R. M. Milburn, J. Am. Chem. Soc. 79, 537 (1957).

13. Schumb, Sherrill, and Sweetser, J. Am. Chem. Soc. 59, 2360 (1937).

14. J. P. Hunt and H. Taube, J. Chem. Physics 19, 602 (1951).

15. R. E. Connick and R. E. Poulsen, University of California, unpublished work.

16. A. W. Adamson and R. G. Wilkins, J. Am. Chem. Soc. 76, 3379 (1954).

17. Bjerrum, Poulsen, and Bjerrum, Acta Chem. Scand. 8, 921 (1954).

18. Connick, Hepler, Hugus, Kury, Latimer, and Tsao, J. Am. Chem. Soc. 78, 1827 (1956).

19. E. Rabinowitch and W. H. Stockmayer, J. Am. Chem. Soc. 64, 335 (1942).

20. H. Olerup, Svensk. Kem. Tidskr. 55, 324 (1943).

21. J. E. Wertz, J. Chem. Physics 24, 484 (1956).

22. Bruce, Norberg, and Weissman, J. Chem. Physics 24, 473 (1956).

23. G. A. Gamlen and D. O. Jordan, J. Chem. Soc. 1953, 1435.